



**D4.12.2: Identification and  
characterization of aerosol sources  
based on offline integration of  
physical and chemical properties  
[B13]**



Deliverable number:	D4.12.2
Work package:	WP4 – Atmosphere
Intermediate Objective:	IO4.6
Deliverable type:	<input checked="" type="checkbox"/> Document, report
	<input type="checkbox"/> Websites, patent filings, videos, etc.
	<input type="checkbox"/> Other: please specify .....
Dissemination level:	<input checked="" type="checkbox"/> Public
	<input type="checkbox"/> Restricted
Estimated delivery (bimester):	B13
Actual delivery date:	28/02/2025
Author(s) (Partner-OU):	Daniele Contini, Daniela Cesari, Adelaide Dinoi, Fabio Massimo Grasso, Antonio Pennetta, Ermelinda Bloise, Paola Semeraro, Florin Unga, Serena Potì, Giuseppe Deluca, Luca Cirillo Ciricugno, Pierina Ielpo, Caterina Mapelli, Francesca Barnaba (CNR-ISAC)
Reviewed by:	Angela Marinoni (CNR-ISAC Bologna)
Note:	

IR0000032 – ITINERIS, Italian Integrated Environmental Research Infrastructures System - CUP B53C22002150006 (D.D. n. 130/2022)  
 Funded by EU - Next Generation EU  
 Mission 4 “Education and Research” - Component 2: “From research to business” -  
 Investment 3.1: “Fund for the realisation of an integrated system of research and innovation infrastructures”

## Table of contents

<i>INTRODUCTION</i> .....	5
<i>INTER-COMPARISON OF ONLINE AND OFFLINE CARBON MEASUREMENTS WITH A FOCUS ON IDENTIFICATION OF SOURCES</i> .....	6
<i>STATUS AND OPERATIVITY OF THE ACSM</i> .....	13
<i>STATUS AND OPERATIVITY OF THE ONLINE ED-XRF SYSTEM (XACT)</i> .....	19
<i>PMF SOURCE APPORTIONMENT BASED ON MEASUREMENTS OF PARTICLE NUMBER CONCENTRATIONS AND COMPARISON WITH CHEMICAL-BASED APPORTIONMENT</i> .....	27
<i>CONCLUSIONS</i> .....	37
<i>REFERENCES</i> .....	37

## Index of Tables

<i>Table 1. Re-calculated MAC values for instruments MAAP, AE33 and Giano BC1. In parenthesis standard errors.</i> .....	10
<i>Table 2. List of the 34 measurable elements, their corresponding LOD values, and the percentage of measurements exceeding the LOD during the analyzed period.</i> .....	20
<i>Table 3. Chemical species and chemical PMF factors correlating with size-PMF factors with <math>R \geq 0.5</math>.</i> .....	35

## Index of Figures

<i>Figure 1. Sampling set-up: the ECO facility (a, b) and the Giano BC1 black carbon analyser (c).</i> ..	7
<i>Figure 2. Daily trend of OC and EC both in PM10 (top) and PM2.5 (bottom) fractions.</i> .....	9
<i>Figure 3. eBC re-calculated from MAAP, AE33 and Giano BC1 versus EC measured with Sunset (EUSAAR2 protocol).</i> .....	11
<i>Figure 4. Daily pattern of eBC (<math>\mu\text{g}/\text{m}^3</math>) measured with MAAP, AE33 and GIANO BC1.</i> .....	11
<i>Figure 5. Daily pattern of OC, SOC and POC (<math>\mu\text{g}/\text{m}^3</math>) obtained by measurement from with TCA.</i> 12	
<i>Figure 6. Daily pattern of eBCff and eBCbb retrieved with Aethalometer model approach.</i> .....	13
<i>Figure 7. Time series in UTC for the different species. In the legend, the corrections made to the raw data are indicated next to the species: AB indicates the correction for the air beam, while CDCE indicates the one related to the Composition Dependent Collect.</i> .....	15
<i>Figure 8. Daily pattern of the organics fraction.</i> .....	16
<i>Figure 9. Daily pattern of nitrate.</i> .....	16
<i>Figure 10. Daily pattern of sulphate.</i> .....	17
<i>Figure 11. Daily pattern of ammonium.</i> .....	17
<i>Figure 12. Daily pattern of chloride.</i> .....	18
<i>Figure 13. Weekly patterns of the different chemical species.</i> .....	18

<i>Figure 14. Average daily pattern of sulphur, silicon, calcium, and titanium. Error bars represent the standard errors.....</i>	<i>20</i>
<i>Figure 15. Average daily patterns of iron chromium, manganese, and barium. Error bars represent the standard errors.....</i>	<i>21</i>
<i>Figure 16. Average daily patterns of potassium, chlorine, strontium, and lead. Error bars represent the standard errors.....</i>	<i>22</i>
<i>Figure 17. Peak concentrations of sulphur, aluminium, barium, and copper recorded during New Year's celebrations. ....</i>	<i>23</i>
<i>Figure 18. Silicon, aluminium, and titanium concentrations during Saharan dust events. ....</i>	<i>24</i>
<i>Figure 19. Atmospheric dust concentration forecasts over the Mediterranean and North African area.....</i>	<i>24</i>
<i>Figure 20. Pollution roses (bivariate plots) showing the distribution of Si, S, Ca, and Ti concentrations as a function of wind direction and wind speed. The radial axis represents wind speed (m/s), while the angular position indicates wind direction. The colour scale represents the concentration of the elements (ng/m<sup>3</sup>), with warmer colour (red) indicating higher concentrations. ....</i>	<i>25</i>
<i>Figure 21. Pollution roses (bivariate plots) showing the distribution of K, Fe, Cu, and Zn concentrations as a function of wind direction and wind speed. The radial axis represents wind speed (m/s), while the angular position indicates wind direction. The colour scale represents the concentration of the elements (ng/m<sup>3</sup>), with warmer colour (red) indicating higher concentrations. ....</i>	<i>26</i>
<i>Figure 22. Monthly resolved median size distributions expressed in number (top figures) and volume (bottom figures) concentrations for the year 2016 (on the left) and 2017 (on the right) coming from SMPS (blue) and OPC (red). The shaded area represents the 25th-75th percentile.....</i>	<i>30</i>
<i>Figure 23. . Factor profiles in terms of percentage contribution to the species sum. For convenience, factor naming follows the dimension of the size bin corresponding to the modal radius.....</i>	<i>31</i>
<i>Figure 24. Percentage contribution to the total eBC for each factor. ....</i>	<i>31</i>
<i>Figure 25. Bar charts display the mean percentage contribution to the total volume (top left) and total number (bottom left) of size bins across the year (grey bars), and separately for cold (October–March, blue bars) and warm (April–September, yellow bars) months. Standard error is indicated by error bars. Additionally, the figure includes particle volume (top right) and number (bottom right) distributions of the 8 factors. ....</i>	<i>31</i>
<i>Figure 26. Hourly, weekly and daily temporal trend of the 8-factor solutions in terms of volume and number concentrations. ....</i>	<i>33</i>
<i>Figure 27. Polar plots for the eight PMF factors. ....</i>	<i>33</i>
<i>Figure 28. Correlation matrix between daily means of size-PMF factors and chemical species determined by Giannossa et al.(2022). ....</i>	<i>34</i>
<i>Figure 29. Correlation matrix between daily means of size-PMF factors and chemical PMF factors determined by Giannossa et al.(2022). ....</i>	<i>35</i>

## INTRODUCTION

This deliverable is prepared in the context of the ITINERIS project, within the Work Package 4 that deals with the integration of Research Infrastructures working in the atmospheric domain through synergistic approaches and cross boundaries developments. The deliverable reports the progress in the source identification by using physical and chemical data of particulate matter with offline analysis (Activity 4.12). Specifically, it will be discussed: how the integration of high temporal resolution measurements of carbon could help in the characterization of biomass burning and traffic sources that may be often mixed in atmosphere, making their discrimination more challenging.

This document is structured in six different chapters: the introduction; four chapters dealing with the above-mentioned aspects; conclusions.

## INTER-COMPARISON OF ONLINE AND OFFLINE CARBON MEASUREMENTS WITH A FOCUS ON IDENTIFICATION OF SOURCES

Carbonaceous aerosols (CA) represent an atmospheric pollutant with critical local, regional, and global importance. CAs can be described by numerous components of different origins. According with the literature, these fractions are commonly indicated by this acronym (Massabò et al., 2021). In the following we reported a brief list of CA acronyms considered in this report:

- TC (Total Carbon) is the total mass of carbon in an aerosol sample. Frequently, TC is measured by thermal evolution or thermo-optical analysis.
- EC (Elemental Carbon) is operationally defined as the fraction of TC carbon which does not volatilize at low temperature, usually below 550°C. EC is a primary pollutant being mainly released in particle-phase from incomplete combustion processes of carbon-containing fuels.
- OC (Organic Carbon) is the fraction of TC containing organic molecules. OC includes thousands of different organic compounds (e.g., aliphatic, aromatic hydrocarbons, carboxylic acids and carboxylic compounds with polar substituent, etc.) with widely varying chemical and physical properties. It can be directly emitted as a primary OC (POC) from many sources including combustion, industrial emissions, geological and natural sources. OC can also form in the atmosphere as secondary OC (SOC), when some volatile and semi-volatile organic compounds are chemically transformed, and the products undergo condensation or nucleation.
- eBC (equivalent Black Carbon) is also defined as the TC fraction which shows a high absorption across a wide spectrum of visible and infrared wavelengths. The acronym eBC is frequently used to identify the results of optical determination of the carbon content in the PM. Many authors suggested that eBC values should be delivered together with a suitable MAC (Mass Absorption Cross-section) for the conversion of light absorption coefficient into mass concentration.

CA has a role in different atmospheric processes such as: radiative forcing (Bond et al., 2013; IPCC, 2021), heterogeneous reactions, cloud formation, and regional visibility degradation, along with their potential adverse impact on human health (Daellenbach et al., 2020; Tomašek et al., 2021; WHO, 2021). The carbonaceous fraction is an important component of PM, generally representing between 20% and 50% of its mass (Kanakidou et al., 2005; Putaud et al., 2010), mainly of anthropogenic origin (Bond and Bergstrom, 2006) and because of its effects, scientific community has increased his attention in this pollutant. An intensive observation campaign has been performed between March and April 2023, collecting in parallel daily samples of PM<sub>10</sub> and PM<sub>2.5</sub> and measuring on these samples OC and EC concentrations. Simultaneously, equivalent black carbon (eBC) concentrations were monitored online by means of three different instruments: a Multi-Angle Absorption Photometer (MAAP), an aethalometer, and a Giano BC1 black carbon analyser. Further information has been also gained measuring online the total carbon (TC). The principal aim of this study was exploring the potentiality of high time resolution measurements of eBC and TC, and their utility in inferring the carbonaceous sources affecting a defined sampling site.

### Measurement site and set-up

The sampling site is at institute CNR-ISAC of Lecce, where is located the Environmental Climate Observatory (named in the following ECO) (SE Italy, 40°20'8" N - 18°07'28" E, 37 m a.s.l.) (Fig. 1a). The study site, classified as an urban background site (Cesari et al., 2018), is subjected to long-range transport phenomena from East Europe and coarse dust advection events from Africa, as well as sea spray contribution and secondary aerosol formation due to photochemical transformation of

air pollutants, thus representing a mix of regional background conditions in the heart of the Mediterranean basin. The sampling set-up used for this study was composed of two automatic aerosol samplers: the SWAM 5A Dual Channel Monitor (FAI Instruments srl), located in the ECO shelter (Figure 1a), providing simultaneously  $PM_{10}$  and  $PM_{2.5}$  mass concentrations according to the  $\beta$ -attenuation method; and the Giano BC1 black carbon analyser, composed of a standard low-volume PM sampler equipped with an optical module for eBC online measurements. The Giano BC1 was installed on the roof of the ISAC building, close to the ECO shelter (Figure 1b). In this report, the PM concentrations used for data analysis are those measured with the SWAM5A Dual Channel Monitor. Between 22 March and 19 April 2023, 86 aerosol samples (57  $PM_{10}$  and 29  $PM_{2.5}$ ) were collected, using quartz fibre filters (Whatmann, 47 mm in diameter). All filters were thermally pre-treated (for 2h at 700°C) to remove, before sampling, any residual carbon contamination on blank membranes (Dinoi et al., 2017). The collected daily PM samples were stored at 4°C until the EC/OC analysis. The analysis of carbonaceous species (i.e. EC/OC) in PM samples were done using a Sunset OC/EC Analyser (Sunset Laboratory Inc., OR, USA, Figure 1b) operating with the EUSAAR2 protocol (thermo-optical method). A multipoint calibration, using as external standard a sucrose solution (2.198 g/l in water, CPAchem Ltd), was done to correct OC and EC measured concentrations. Linear calibration had a slope of 0.97, a negligible intercept, and a determination coefficient  $R^2=1$ .

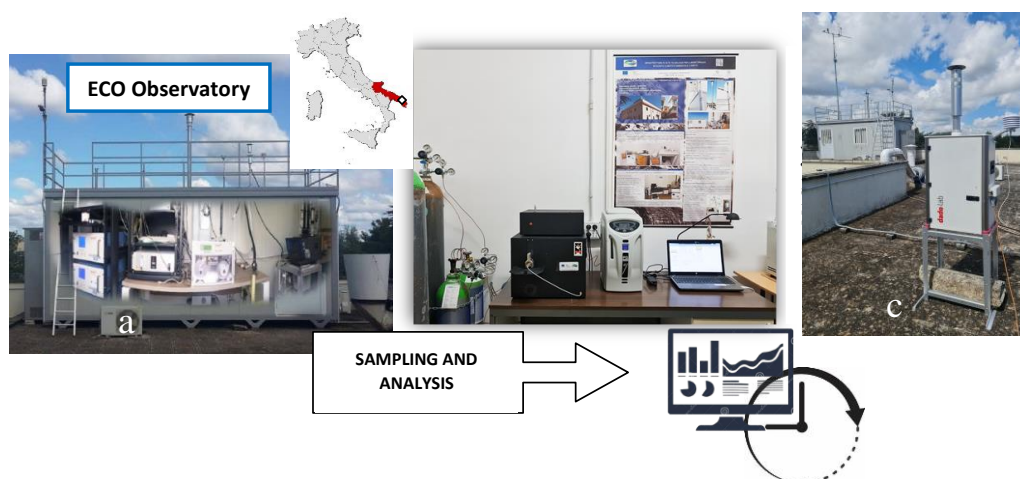


Figure 1. Sampling set-up: the ECO facility and the Giano BC1 black carbon analyser.

In measurements of eBC, the Mass Absorption Cross-section (MAC) is an important parameter to describe the optical properties of EC (Liu et al., 2015). MAC has been firstly introduced by Bond et al. (2006) as the light absorption cross section normalized to the mass of a given species (e.g. BC) of aerosol particles (in units of  $m^2/g$ ) both for absorption or scattering cross section, and is applied for the conversion of the light absorption coefficient to eBC mass concentration. Commercial instruments typically use a predefined fixed MAC value, which does often not agree with the MAC value of the sampled aerosol, bringing to discrepancies between eBC and EC measurements. Zanatta et al. (2016) reported MAC values found in European ACTRIS network, which ranged between 4.3 and 22.7  $m^2/g$  at a wavelength of 637 nm. Recent studies highlighted the need of harmonization of all involved methods and instruments during extensive inter-comparison exercises, in order to get a

more realistic picture in determining MAC or eBC (Savadkoochi et al., 2023). Regarding the eBC online measurements in ECO site, these data were obtained using four instruments:

- A MAAP (Thermoscientific, mod. 5012), equipped with a PM<sub>10</sub> head, operating at a wavelength of  $\lambda=637$  nm (Petzold et al., 2002). The instrument's algorithm converts the fraction of light absorption by adsorbing aerosol components (via a radiative transfer program) to mass concentration of eBC, using a pre-defined value of the Mass Absorption Cross-section (MAC 6.6 m<sup>2</sup>/g), specific at the measurement wavelength.
- An aethalometer (MAGEE AE33), located inside the ECO shelter, is equipped with a PM<sub>2.5</sub> head, and 7 lamps which allowed to estimate the absorption Ångström exponent by means of a best-fit procedure, as described in Esposito et al. (2012). The fraction of light absorption by adsorbing aerosol components is converted to mass concentration of eBC using a pre-defined value of MAC, at the measurement wavelength of 880 nm. Furthermore, the use of multi-wavelength Aethalometer data, like those retrieved from AE33, may be also used to derive the traffic and the wood-burning contributions to eBC.
- A Giano BC1 black carbon analyser (Dadolab Srl) equipped with a PM<sub>10</sub> head. Also this instrument converts the fraction of light absorption by adsorbing aerosol components to mass concentration of eBC, using a pre-defined value of MAC, specific at the measurement wavelength of 635 nm.

Further information regarding carbonaceous aerosol could be gained by a Real Time Total Carbon Aerosol Analyzer (Aerosol Magee Scientific, TCA08) located in the ECO observatory. This instrument, equipped with a PM<sub>2.5</sub> head, uses a thermal method for TC determination. It is composed of two parallel flow channels with two analytical chambers, which alternate between sample collection and thermal analysis, giving a semi-continuous TC measurement. Further, it is possible obtain the concentration of organic carbon (OC) by subtracting black carbon concentration measured by the AE33, from the total carbon concentration measured by the TCA08.

#### Determination of specific MAC in ECO site

In this study, the actual MAC for the specific ECO site was calculated (Baumgardner et al., 2012; Bond et al., 2013; Zanatta et al., 2016). Knowing that the MAC used in each instrument at a defined measurement wavelength ( $\lambda$ ), is a predefined constant value to infer eBC<sub>raw</sub> mass concentration (in  $\mu\text{g}/\text{m}^3$ ) from light absorption coefficient measurements ( $\sigma_{\text{abs}}$ ). For example, in MAAP where MAC is 6.6 m<sup>2</sup>/g at the measurement wavelength of 670nm, we have:

$$\text{eBC}_{\text{raw}} = \sigma_{\text{abs},670 \text{ nm}} / 6.6 \quad (\text{Eq. 1})$$

$$\text{MAC} = \sigma_{\text{abs},670 \text{ nm}} * (1/\text{CF}) / (\text{EC} * 10^6) = \sigma_{\text{abs},637 \text{ nm}} / (\text{EC} * 10^6) \quad (\text{Eq. 2})$$

$$\text{eBC} = \sigma_{\text{abs},637 \text{ nm}} / \text{MAC} * 10^6 \quad (\text{Eq. 3})$$

Where CF=0.952 is a conversion factor applied to the firmware output of the MAAP, to obtain the absorption coefficient at 637 nm (Müller et al., 2011). This approach has been applied also for calculating the new MAC of AE33 and of Giano BC1, having a pre-imposed value of 7.77 m<sup>2</sup>/g ( $\lambda=$

880nm) and  $10 \text{ m}^2/\text{g}$  ( $\lambda = 635\text{nm}$ ) respectively. For AE33 the harmonization SOP of ACTRIS was used.

Determination of POC and SOC from TCA data

Data collected with the TCA08 analyser allowed the determination of the secondary organic carbon (SOC) and of the primary organic carbon (POC), following the method described in Ivančič et al., (2022) and assuming that POC and BC are co-emitted by combustion sources. The equations are:

$$\text{POC} = (\text{OC}/\text{BC})_{\text{prim}} \times \text{BC} \quad (\text{Eq. 4})$$

$$\text{SOC} = \text{OC} - \text{POC} \quad (\text{Eq. 5})$$

For calculating the ratio  $(\text{OC}/\text{BC})_{\text{prim}}$ , the R-squared method has been used. Briefly, the hypothetical SOC is firstly calculated for a wide range of hypothetical  $(\text{OC}/\text{BC})_{\text{prim}}$  ratios (for ratios 0.1 to 10 in 0.1 steps). SOC and BC is calculated for every hypothetical  $(\text{OC}/\text{BC})_{\text{prim}}$  ratio, and the optimal  $(\text{OC}/\text{BC})_{\text{prim}}$  ratio is chosen where the R-squared is minimal. In Figure 2 a summary of  $\text{PM}_{10}$  and  $\text{PM}_{2.5}$  measurements together with OC/EC thermo-optic determination is reported for the studied period.

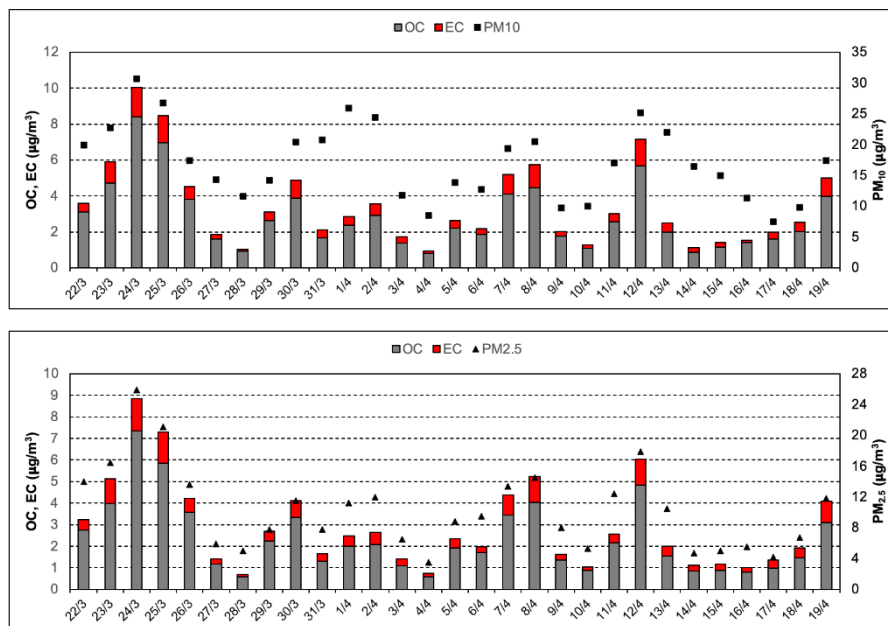


Figure 2. Daily trend of OC and EC both in  $\text{PM}_{10}$  (top) and  $\text{PM}_{2.5}$  (bottom) fractions.

The average concentrations of PM obtained were  $17.1 (\pm 1.1) \mu\text{g}/\text{m}^3$  for  $\text{PM}_{10}$  and  $10.4 (\pm 1.0) \mu\text{g}/\text{m}^3$  for  $\text{PM}_{2.5}$ . Considering the whole measurement period, OC and EC represented, on average, 16.5% and 3.6 % of  $\text{PM}_{10}$  in mass, and 22.6% and 5.5% of  $\text{PM}_{2.5}$ . These values are in agreement with those reported in a recent study of Merico et al., (2025). The complete dataset of eBC raw data, collected

with MAAP, AE33 and Giano BC1, and EC concentration, obtained with the Sunset (EUSAAR2 protocol), were used to estimate the MAC in-situ. In Table 1, the new values of MAC are reported.

<i>Instrument</i>	<i>MAC (m<sup>2</sup>/g)</i>
MAAP	12.04 (0.26)
AE33	8.08 (0.33)
Giano BC1	12.22 (0.47)

*Table 1. Re-calculated MAC values for instruments MAAP, AE33 and Giano BC1. In parenthesis standard errors.*

Comparing these values with those obtained in the work of Zanatta et al. (2016), where the MAC for several European sites (mediterranean and continental Europe background) was found, showing a range between  $8.92 \pm 1.65$  m<sup>2</sup>/g and  $17.3 \pm 1.71$  m<sup>2</sup>/g and a geometric mean value of  $10 \pm 1.3$  m<sup>2</sup>/g. Also the work of Savadkoochi et al. (2024) investigated the MAC at different typologies of sites (urban background, rural, and traffic) in Europe. A comparison of the MAC found here with the results of urban background sites showed the comparability of the results at ECO with the range (10-14 m<sup>2</sup>/g) observed by Savadkoochi et al. (2024). Other studies conducted at the wavelength of 637 nm with MAAP instrument, estimated comparable MAC values of  $10.4 \pm 0.2$ ,  $10.9 \pm 3.5$  and  $10.2 \pm 3.2$  m<sup>2</sup>/g, for regional background (Pandolfi et al., 2011), remote mountaintop (Pandolfi et al., 2014), rural high alpine sites (Liu et al., 2010), respectively. This confirmed the limited spatial variability of MAC, oppositely with chemical and physical transformations of BC (i.e., aging) in atmosphere, that could influence BC light absorption (Yuan et al., 2021; Zanatta et al., 2016; Sun et al., 2020).

The comparison of the re-calculated eBC daily concentrations from MAAP, AE33 and Giano BC1 and the EC data concentrations resulted in good agreement, with observed R<sup>2</sup> greater than 0.97 for all instruments (Figure 3). It is worth noting that after introduction of the new MAC, some differences between eBC (optically measured) and thermo-optically measured EC could be due to various causes not arising to the used MAC, for example: charring of OC in thermo-optical analysis (Chow et al., 2004); thermal protocol used, that determines different split points (Merico et al., 2019); presence of

BrC, related to biomass burning activities, that could lead to higher eBC measurements by the MAAP (Andreae and Gelencsér, 2006).

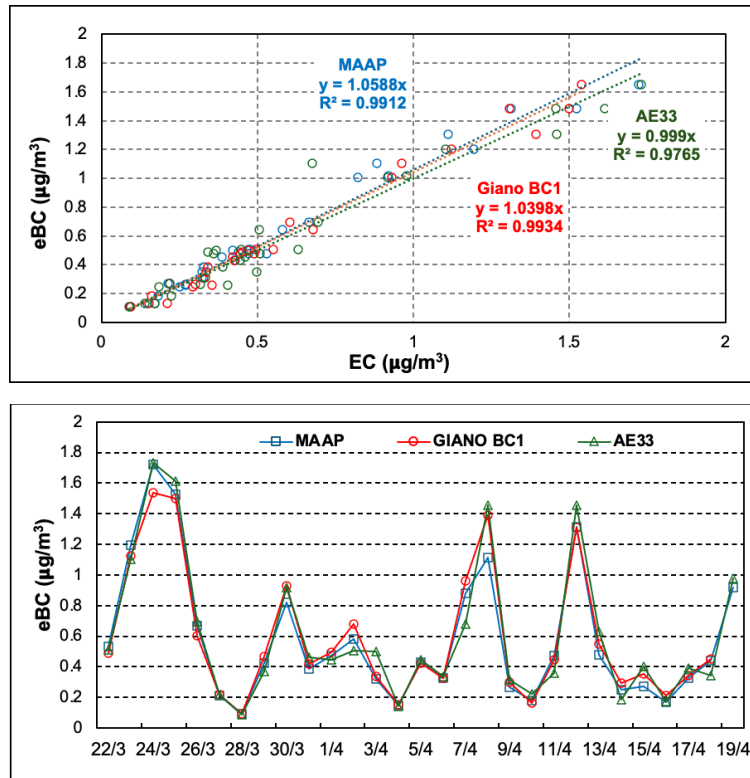


Figure 3. eBC re-calculated from MAAP, AE33 and Giano BC1 versus EC measured with Sunset (EUSAAR2 protocol).

In Figure 4 the daily pattern of eBC, measured with MAAP, AE33 and GIANO BC1, is reported. The daily pattern shows some interesting aspects. The first is that the lowest concentrations are observed around midday and early afternoon and there is a clear modulation of the atmospheric eBC concentrations due to the daily evolution of the planetary boundary layer (PBL) height. The second aspect is that in the early morning a peak is evident, probably due to traffic emissions, which occurs at 6 am. Finally, during the evening/nighttime there is a eBC peak higher that is probably due to a mixed effect between the PBL dynamics and the traffic and domestic heating emissions.

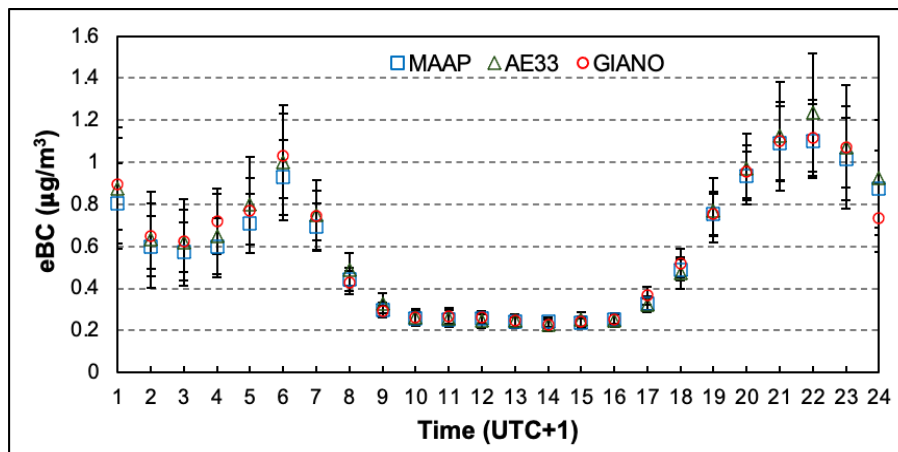


Figure 4. Daily pattern of eBC ( $\mu\text{g}/\text{m}^3$ ) measured with MAAP, AE33 and GIANO BC1.

In Figure 5 the OC daily concentration obtained by TCA measurements is reported together with secondary organic carbon and primary organic carbon concentrations. POC and SOC concentrations are not directly measured but calculated according equations 4 and 5. The  $(OC/EC)_{prim}$  obtained for the considered period was 2.9 and is very close to the values reported by Merico et al. (2025), who observed an  $(OC/EC)_{prim}$  of 2.4 and 2.1 for  $PM_{10}$  and  $PM_{2.5}$ , respectively, during the cold period. On average, the SOC, representing the 36% of the measured OC, has not a daily pattern, having a concentration close to  $1 \mu g/m^3$  the whole day, except for the early morning, where the lowest value is observed at 6 a.m., according with the previous observation reporting that at 6 a.m. a peak of eBC is evident due to traffic emission (Figure 4). Further, the primary organic carbon is characterized by the same daily pattern observed for eBC, confirming then the primary origin of the eBC. In Figure 6 the biomass burning contribution to eBC measured with AE33 is reported together with the fossil fuel contribution. As already mentioned, multi-wavelength Aethalometer data may be used to derive the fossil fuel and the biomass burning contributions to eBC (eBC<sub>ff</sub> and eBC<sub>bb</sub>, respectively). This approach is called “Aethalometer model” and assumes that light-absorbing particles only originate from vehicle and biomass-burning emissions (Sandradewi et al., 2008; Zotter et al., 2017). Results showed that, on average, eBC<sub>ff</sub> accounted for about 65% of the measured eBC, while the eBC<sub>bb</sub> is only 35%, indicating that the ECO site is more influenced by fossil fuel combustion in spring season. The analysis of the daily pattern showed two pronounced peaks for eBC<sub>ff</sub>: the former in the early morning at 6 a.m., the second in the evening at 22 p.m., clearly associated with human activity, traffic emissions in particular. As previously stated, the nighttime peak could be due to a combined effect of traffic emissions and the PBL height. Regarding the eBC<sub>bb</sub> daily pattern, this is mainly characterized by a peak during the evening/night, less pronounced than that of eBC<sub>ff</sub>, that could be due both to the use of biomass burning for domestic heating and a to the PBL dynamic.

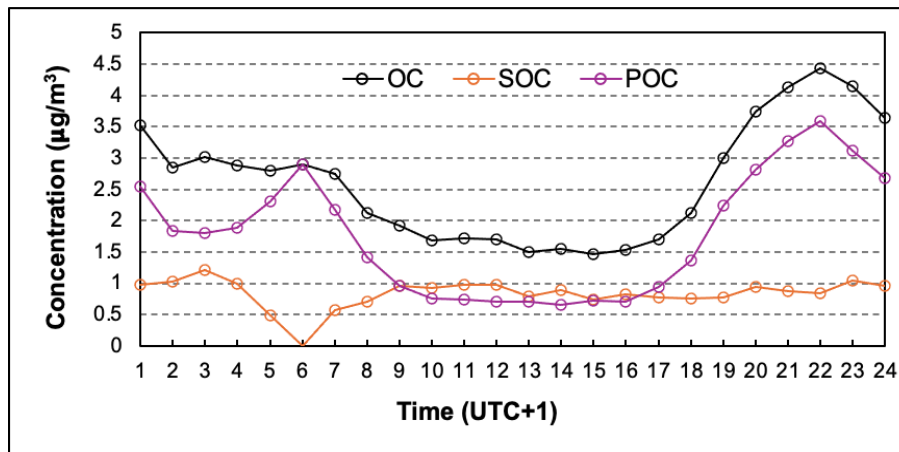


Figure 5. Daily pattern of OC, SOC and POC ( $\mu g/m^3$ ) obtained by measurement from with TCA.

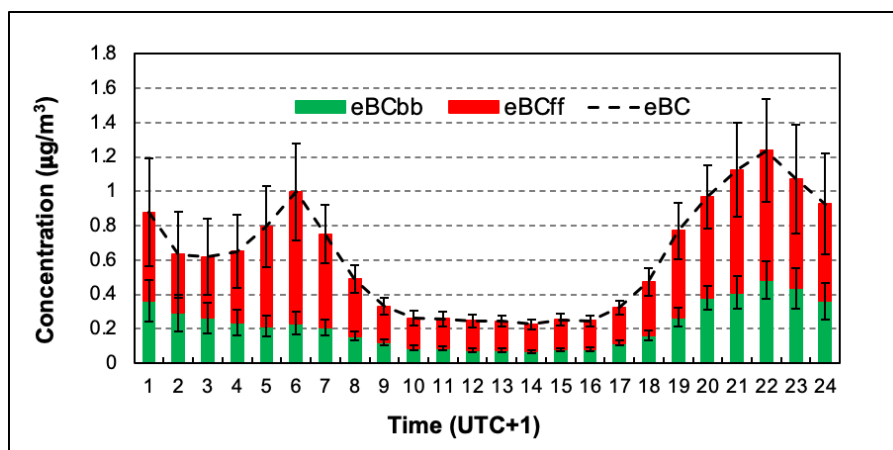


Figure 6. Daily pattern of eBCff and eBCbb retrieved with Aethalometer model approach.

## Summary

- An intensive observatory campaign has been performed between March and April 2023, collecting in parallel daily samples of PM<sub>10</sub> and PM<sub>2.5</sub>, determining their content in OC and EC concentrations and simultaneously, collecting in high time resolution eBC and TC data.
- The average concentrations of PM obtained were 17.1 ( $\pm$  1.1)  $\mu\text{g m}^{-3}$  for PM<sub>10</sub> and 10.4 ( $\pm$  1.0)  $\mu\text{g m}^{-3}$  for PM<sub>2.5</sub>. Considering the whole measurement period, OC and EC represented, on average, 16.5% and 3.6 % of PM<sub>10</sub> in mass, and 22.6% and 5.5% of PM<sub>2.5</sub>. These values are in agreement with those reported in a recent study of Merico et al., (submitted).
- The value of MAC in-situ was estimated for the three instruments and was ranging between  $8.0\pm 0.33$  m<sup>2</sup>/g and  $12.22\pm 0.47$  m<sup>2</sup>/g, in agreement with values found for other different typologies of sites in Europe.
- High time resolution measurements allowed to study the pattern of eBC for the ECO site, showing that there is a clear modulation of the atmospheric eBC concentrations due to the daily evolution of the planetary boundary layer (PBL) height. Further the ECO site is influenced by combustion sources, mainly by traffic emissions, as evidenced by apportionment of eBC in 65% of eBC<sub>ff</sub> and 35% of eBC<sub>bb</sub>, with a main peak observed in the early morning associated to traffic emissions and a lower peak during the evening/nighttime probably due to a mixed effect between the PBL dynamics, traffic and domestic heating emissions. Finally the SOC was accounting for 36% of the measured OC, and has not a daily pattern, having a concentration close to 1  $\mu\text{g m}^{-3}$  the whole day.

## STATUS AND OPERATIVITY OF THE ACSM

The Aerosol Chemical Speciation Monitor TOF-ACSM089 was installed in the new shelter of ECO station in September 2024. Here the preliminary data analysis of the period 24/09/2024-08/11/2024 is reported. The instrument can furnish measurements at high temporal resolution (10 minutes) of some chemical components of PM<sub>1</sub> and it could furnish information useful for near-real-time source apportionment and for source identification.

The acquired data were validated according to the methodology reported in the Tofware user guide for Tof ACSM manual (updated July 2023 – Aerodyne). Figure 7 shows the time series in UTC of

the data from 24 September to 8 November 2024 for the following species: Organics (Org), nitrate ( $\text{NO}_3$ ), sulphate ( $\text{SO}_4$ ), ammonium ( $\text{NH}_4$ ) and chloride (Chl).

Figures 8, 9, 10, 11, and 12 show the daily patterns of the different measured components. It is observed that organics have a daily pattern comparable to that of OC with lower values during diurnal hours. The same applies for nitrate; while sulphate and ammonium have limited daily variabilities. Figure 13 shows weekly patterns of the different chemical species.

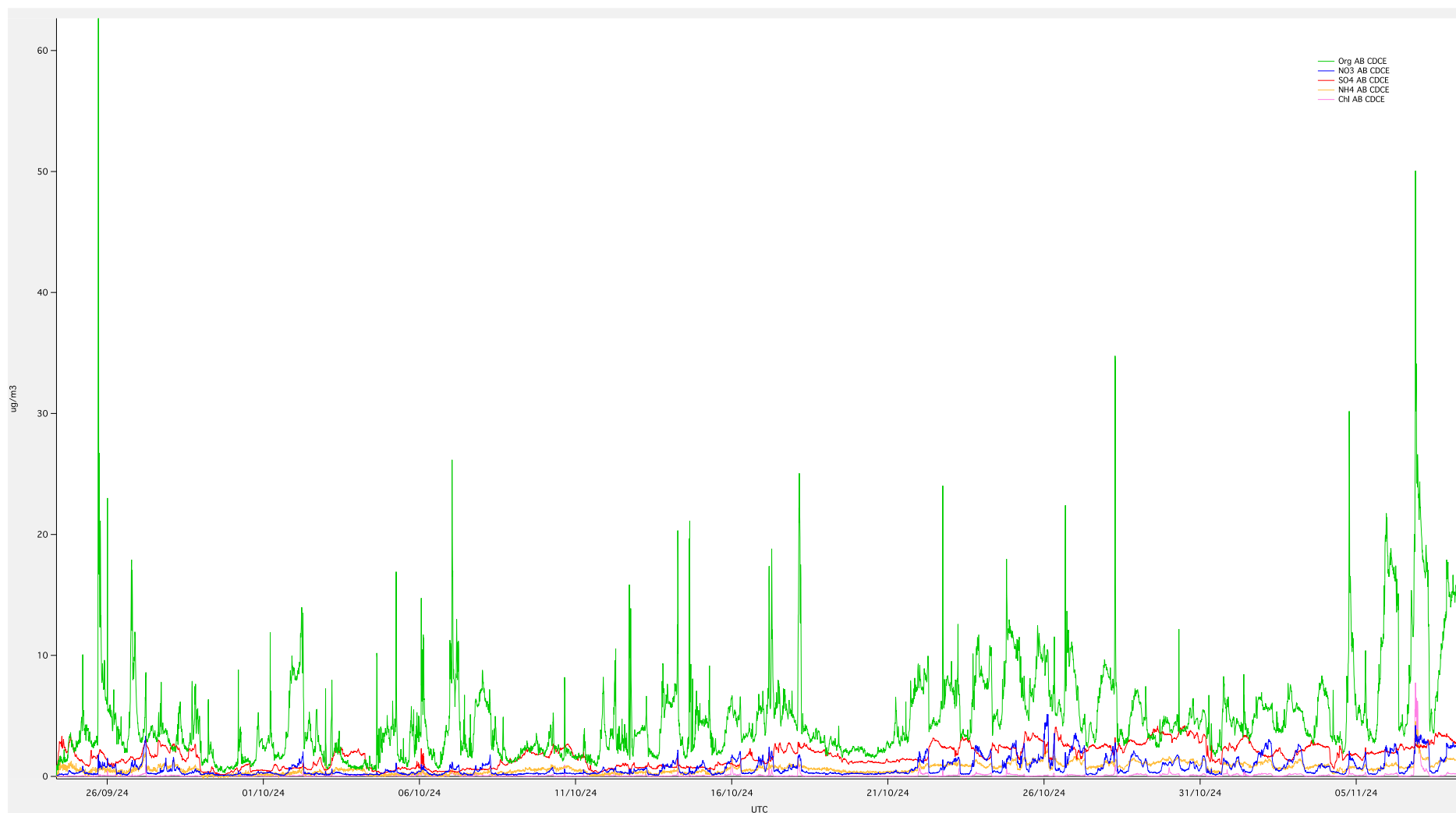


Figure 7. Time series in UTC for the different species. In the legend, the corrections made to the raw data are indicated next to the species: AB indicates the correction for the air beam, while CDCE indicates the one related to the Composition Dependent Collect.

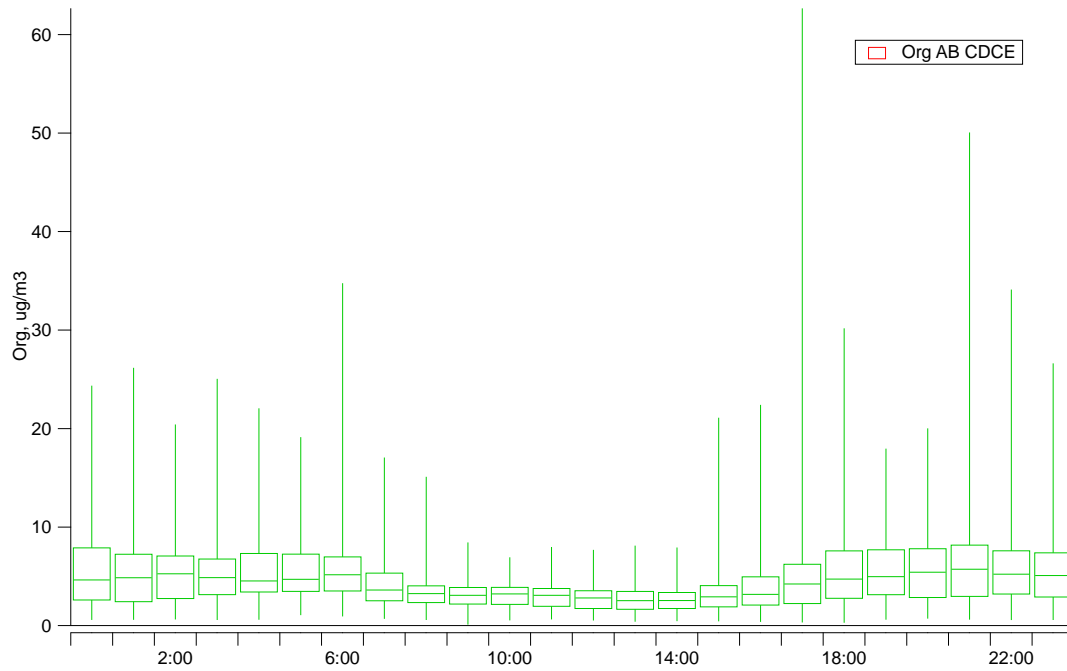


Figure 8. Daily pattern of the organics fraction.

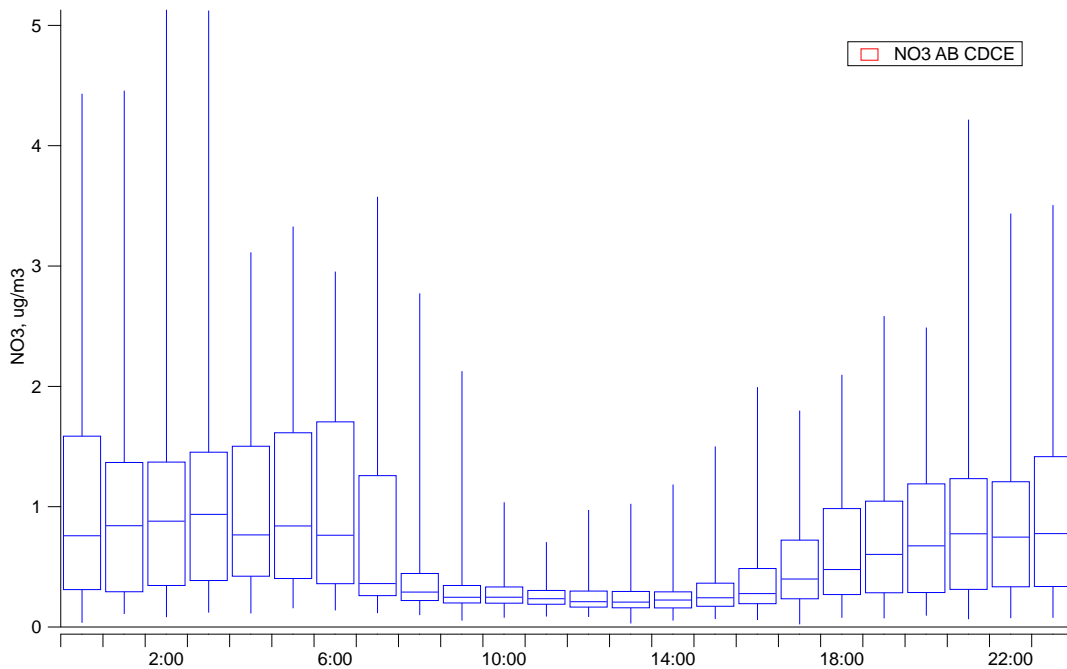


Figure 9. Daily pattern of nitrate.

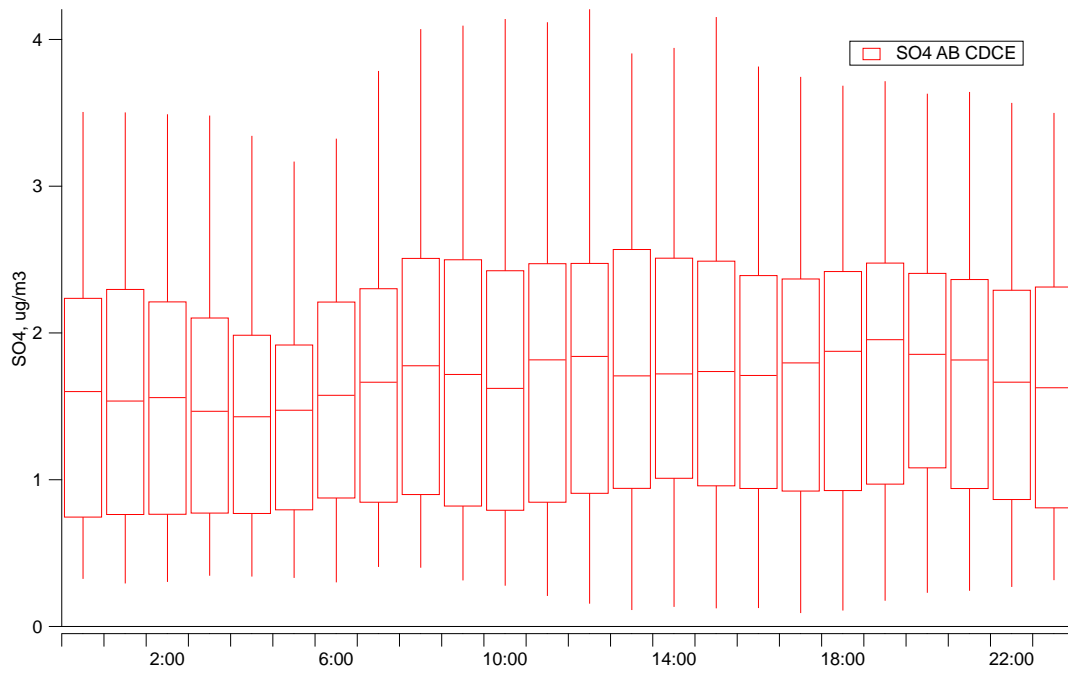


Figure 10. Daily pattern of sulphate.

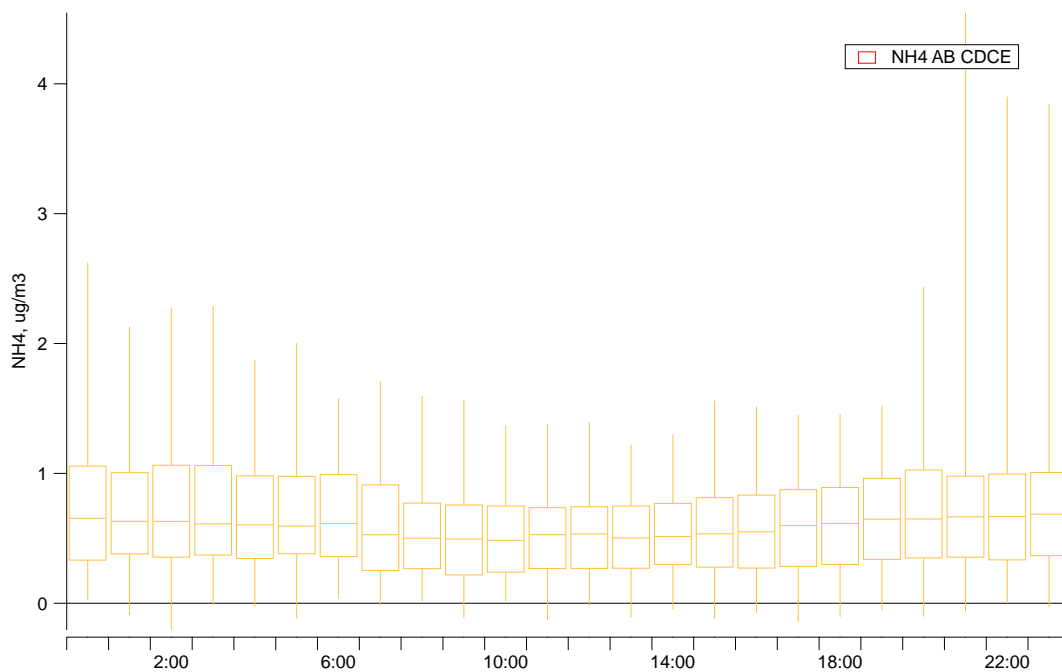


Figure 11. Daily pattern of ammonium.

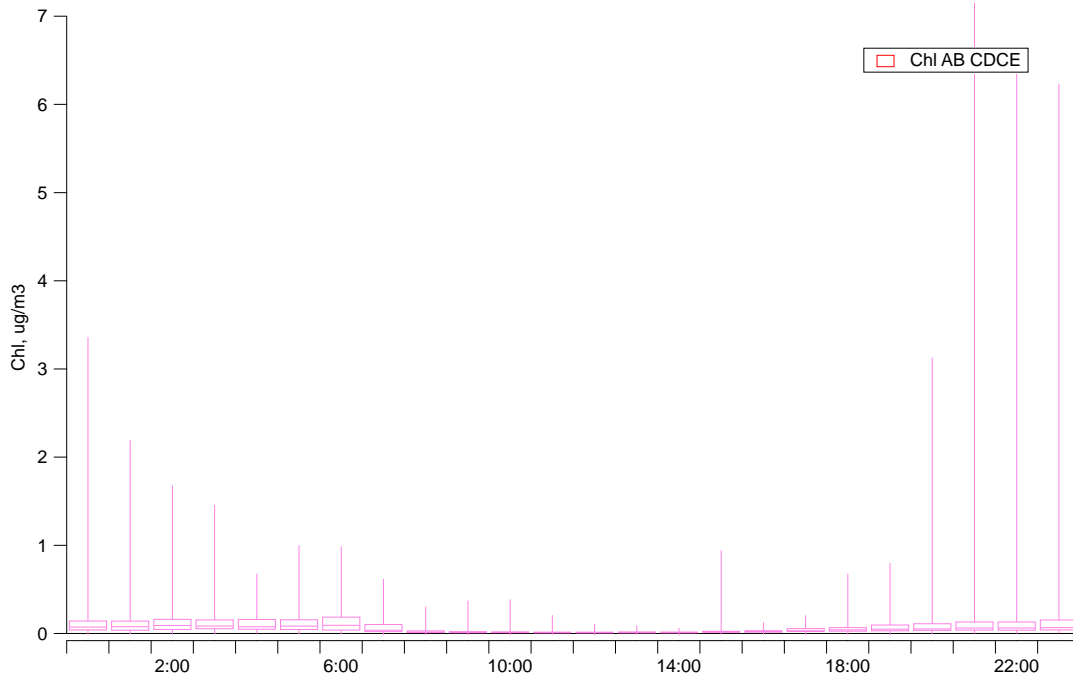


Figure 12. Daily pattern of chloride.

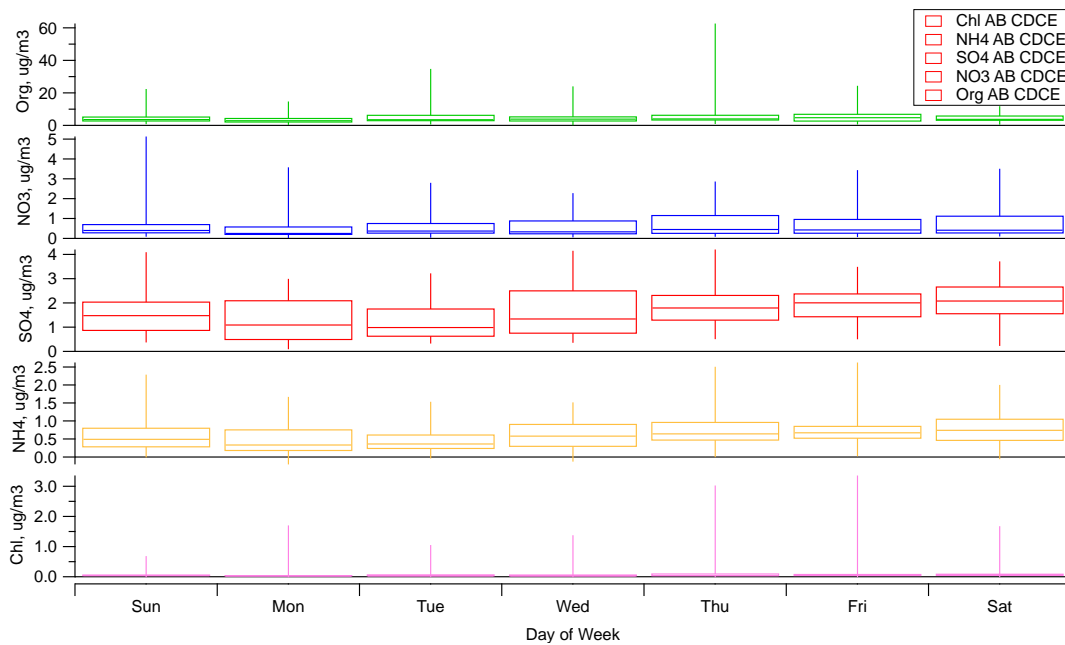


Figure 13. Weekly patterns of the different chemical species.

## STATUS AND OPERATIVITY OF THE ONLINE ED-XRF SYSTEM (XACT)

The Xact® 625i instrument has been installed at ECO (new shelter) for online detection of the elemental chemical composition of atmospheric PM<sub>10</sub> that could provide valuable insights into the nature of its emission sources. In this context, the ECO laboratory, through the ITINERIS project, has acquired an Xact® 625i analyser, specifically designed for near real-time monitoring of metal concentrations in ambient air. This instrument offers high temporal resolution and detection limits comparable to traditional offline laboratory analyses for the majority of the elements. The Xact® 625i is equipped with a meteorological station that records wind speed and direction. Sampling is performed using a PM10 inlet with an operational flow rate of 16.7 L/min. The instrument is calibrated for 44 elements: *Al, Si, P, S, Cl, K, Ca, Ti, V, Cr, Mn, Fe, Co, Ni, Cu, Zn, Ga, Ge, As, Se, Br, Rb, Sr, Y, Zr, Mo, Pd, Ag, Cd, In, Sn, Sb, Te, Cs, Ba, La, Ce, W, Pt, Au, Hg, Tl, Pb e Bi*. A 3-hour sampling interval was chosen to enhance measurement sensitivity. Under the typical conditions of the observatory, not all calibrated species are effectively quantified above the detection limits. Below are the preliminary results from the first measurement period, spanning from 30/11/2024 to 15/02/2025, based on approximately 650 collected data points. Table 2 presents the 34 measurable elements and their corresponding limit of detection (LOD) values, considering a sampling time of 3 hours. The third column indicates the percentage of measurements exceeding the LOD during the analyzed period.

Elements	LOD (ng/m <sup>3</sup> )	Data Above LOD (%)
Aluminium (Al)	19	100
Silicon (Si)	3.4	81
Sulphur (S)	0.6	100
Chlorine (Cl)	0.33	100
Potassium (K)	0.22	100
Calcium (Ca)	0.057	100
Titanium (Ti)	0.03	100
Vanadium (V)	0.023	77
Chromium (Cr)	0.022	94
Manganese (Mn)	0.027	97
Iron (Fe)	0.033	100
Cobalt (Co)	0.026	0
Nickel (Ni)	0.018	99
Copper (Cu)	0.015	100
Zinc (Zn)	0.013	100
Gallium (Ga)	0.011	21
Germanium (Ge)	0.011	0
Arsenic (As)	0.012	99
Selenium (Se)	0.016	86
Bromine (Br)	0.02	100
Strontium (Sr)	0.041	99
Molybdenum (Mo)	0.092	0
Palladium (Pd)	0.42	0
Silver (Ag)	0.37	100

Cadmium (Cd)	0.48	17
Tin (Sn)	0.78	4
Antimony (Sb)	0.99	3
Barium (Ba)	0.074	81
Lanthanum (La)	0.069	0
Platinum (Pt)	0.023	0
Mercury (Hg)	0.023	0
Thallium (Tl)	0.022	0
Lead (Pb)	0.024	84
Bismuth (Bi)	0.025	9

Table 2. List of the 34 measurable elements, their corresponding LOD values, and the percentage of measurements exceeding the LOD during the analyzed period.

During the measurement period, 21 elements recorded at least 75% of concentrations above the LOD. These real-time measurements enhance the capability to identify and characterize atmospheric pollution sources, supporting environmental monitoring and regulatory compliance efforts. The dataset available until end of January was used to identify some characteristics of the primary emission sources impacting the ECO observatory. Figure 14 shows the average daily pattern of sulphur, silicon, calcium, and titanium, elements typically associated with crustal phenomena and secondary inorganic aerosol, which do not exhibit significant daily variability.

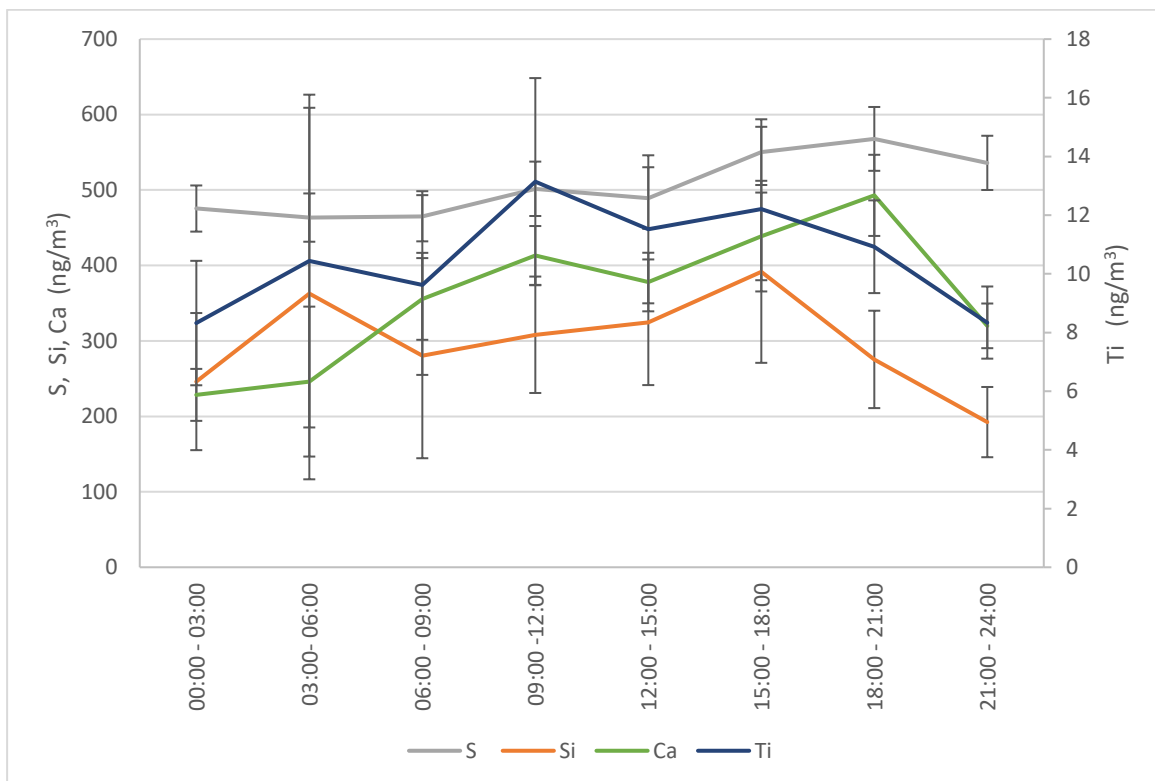


Figure 14. Average daily pattern of sulphur, silicon, calcium, and titanium. Error bars represent the standard errors.

Conversely, Figure 15 presents the daily patterns of iron, chromium, manganese, and barium, whose concentrations fluctuate throughout the day, showing two peaks in the same period of the day in which peaks of primary organic carbon and eBC<sub>ff</sub> (morning) and eBC<sub>bb</sub> (night) suggesting that both combustion sources (i.e. road traffic and biomass burning) influences these elements.

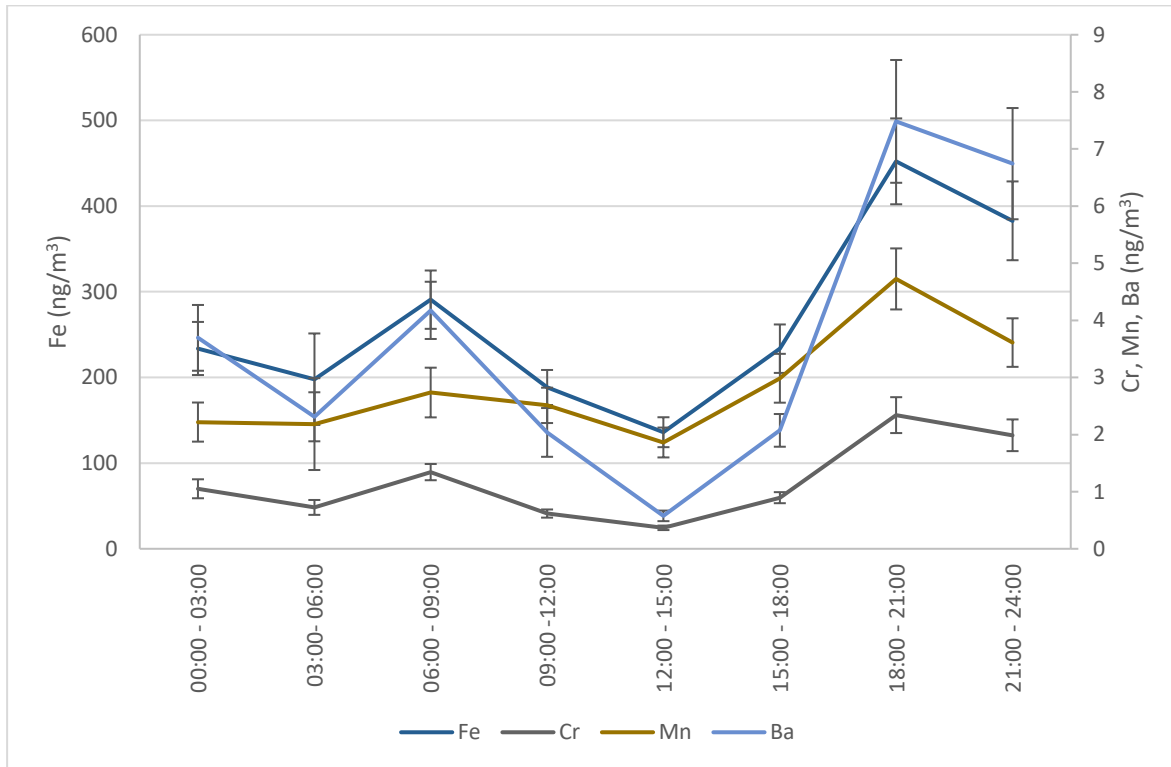


Figure 15. Average daily patterns of iron chromium, manganese, and barium. Error bars represent the standard errors.

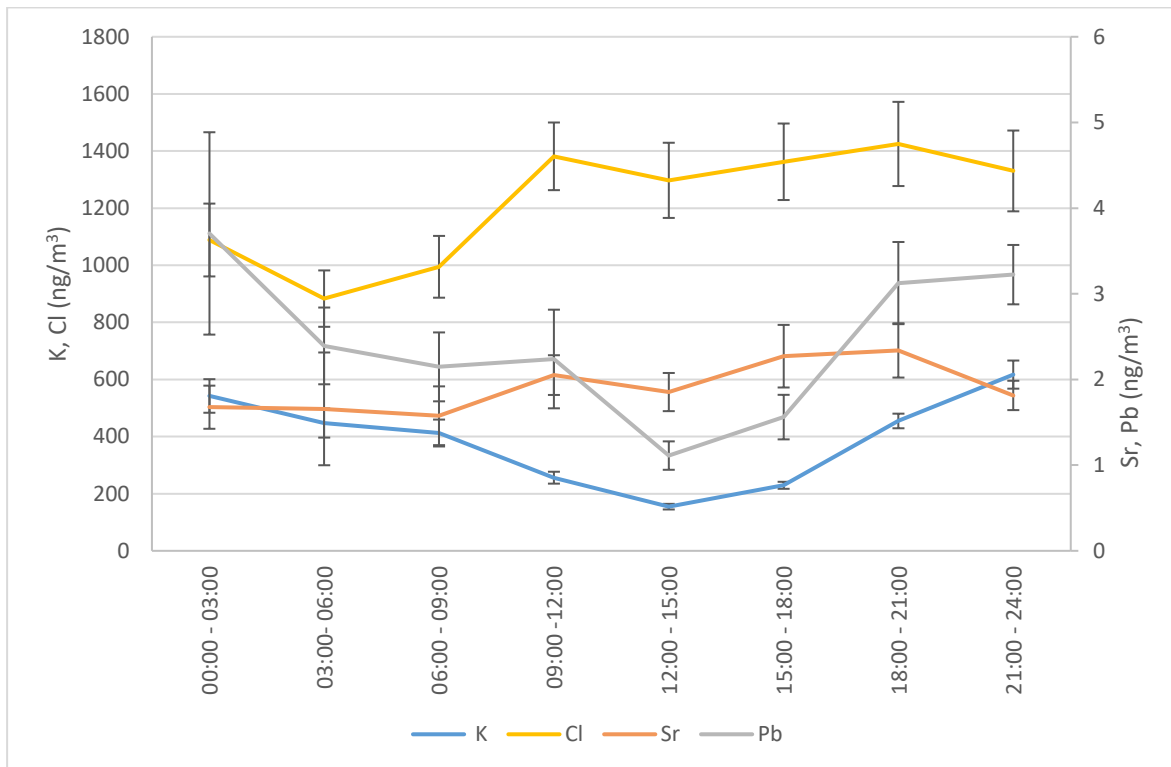


Figure 16. Average daily patterns of potassium, chlorine, strontium, and lead. Error bars represent the standard errors.

The daily pattern of chlorine and strontium is well correlated suggesting possible common sources with an increase during evening and night. Instead, the daily pattern of potassium and lead show a minimum during diurnal hours and an increase in nocturnal concentrations suggesting an influence of the boundary-layer height and of biomass burning.

Additionally, sporadic events were observed on January 1, 2025, associated with fireworks, during which peaks of typical elements such as S, Al, Ba, Bi, and Cu were recorded (see Figure 16). Many elements are used in fireworks as colour or sparkle emitters (e.g.: Al and Mg for white, Ba for green, Cu for blue, Sr for yellow) and have often been used as tracers of this source (Vecchi et al., 2008), even if they are not selective as they are also contained in soil/road dust and nonexhaust traffic emission. In the case of Bi, instead, fireworks are by far the most relevant atmospheric source of this element and its insoluble fraction constitutes a reliable and robust tracer of fireworks (Perrino et al., 2011).

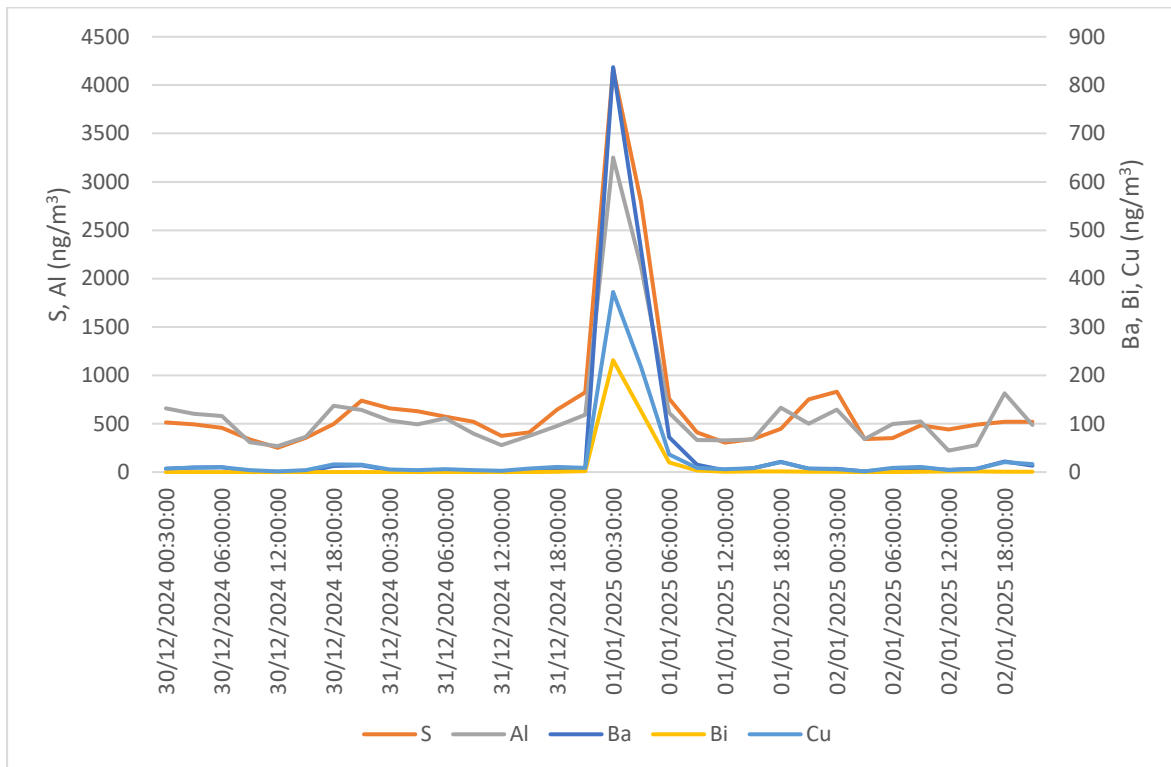


Figure 17. Peak concentrations of sulphur, aluminium, barium, and copper recorded during New Year's celebrations.

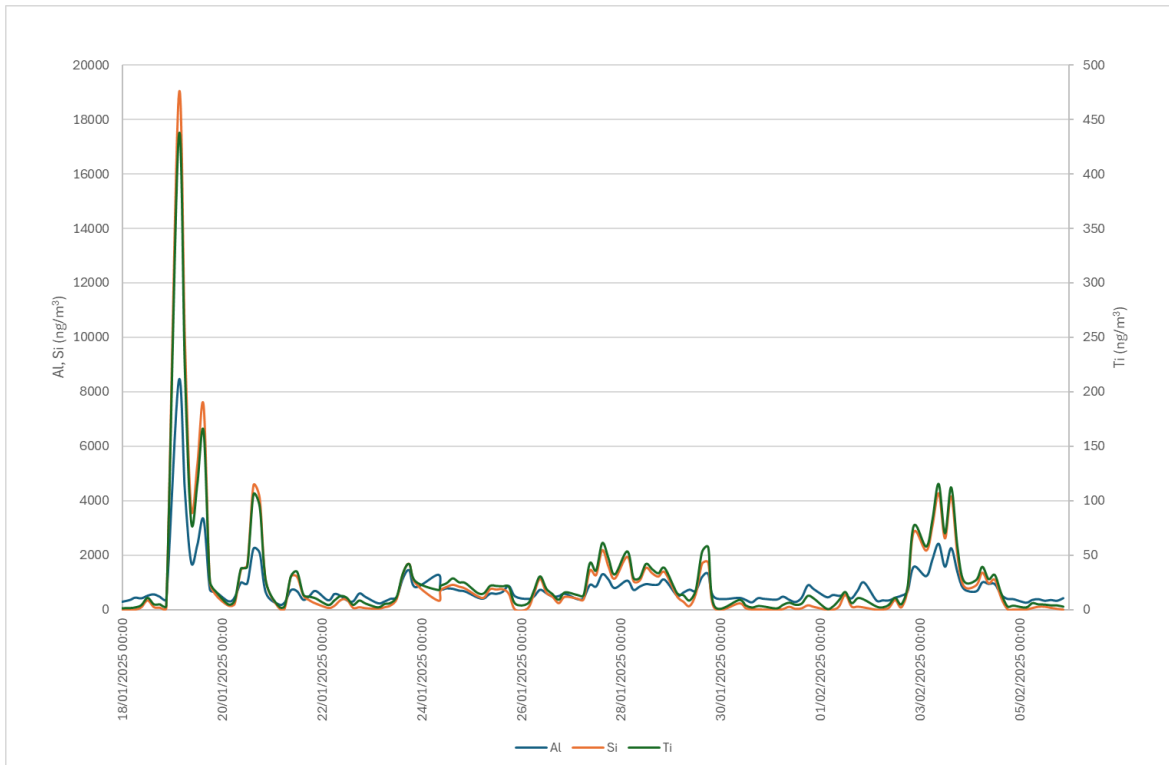


Figure 18. Silicon, aluminium, and titanium concentrations during Saharan dust events.

On January 19-20, 2025, instead, elements such as silicon, aluminium, and titanium showed correlated peaks (Figure 17), likely due to Saharan dust events. Saharan dust events have been confirmed by the dust forecasting and monitoring system developed by AEMET and the Barcelona Supercomputing Center (<https://dust.aemet.es>), which provides daily analyses and predictions of atmospheric dust concentrations over Europe and surrounding regions. Figure 18 presents two plots showing forecasts of Saharan dust transport towards southern Europe, with a particular impact on the Salento region (Apulia), which occurred on January 19 and February 3, 2025. The peaks on February 3 are less intense compared to the previous ones.

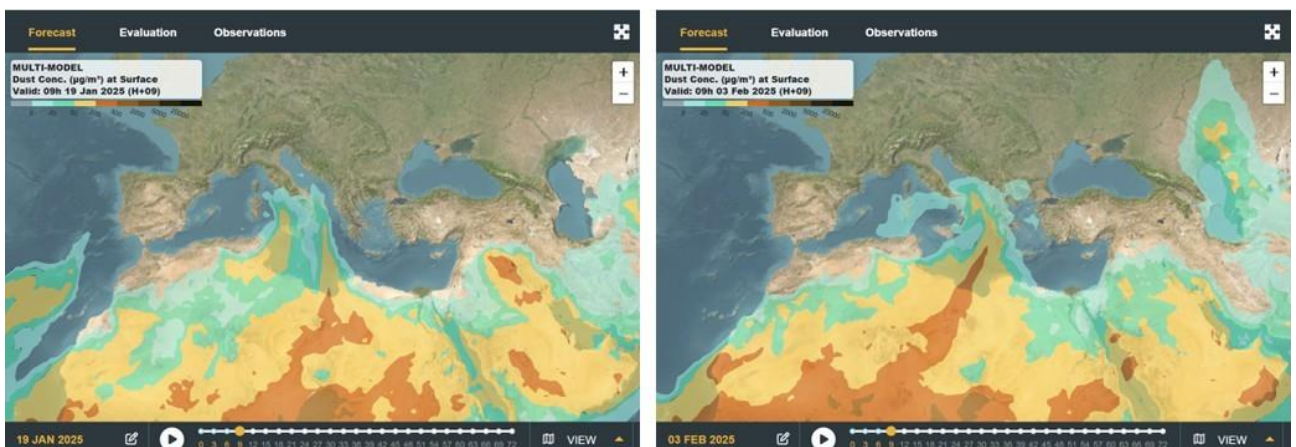


Figure 19. Atmospheric dust concentration forecasts over the Mediterranean and North African area.

The dataset was refined by removing data associated with sporadic events, such as New Year's celebrations and Saharan dust events. By correlating wind speed, direction, and element concentration over a three-hour period, it is possible to generate Bivariate Polar Plots like those shown in Figures 19 and 20, which correspond to elements of crustal and anthropogenic origin, respectively. Figure 19 presents the results of elements typically associated with crustal sources (silicon, calcium, and titanium) and secondary inorganic aerosol (sulphur). The crustal elements are characterized by having remote emission sources relative to the sampling site, as their atmospheric concentrations increase with wind speed. Furthermore, they exhibit a consistent pattern in which the highest concentrations are recorded under southerly wind conditions. Sulphur shows a more complex pattern with high concentrations observed also during N-NE winds and even contributions at low wind speed suggesting that secondary sulphate comes from different sources and regional contributions.

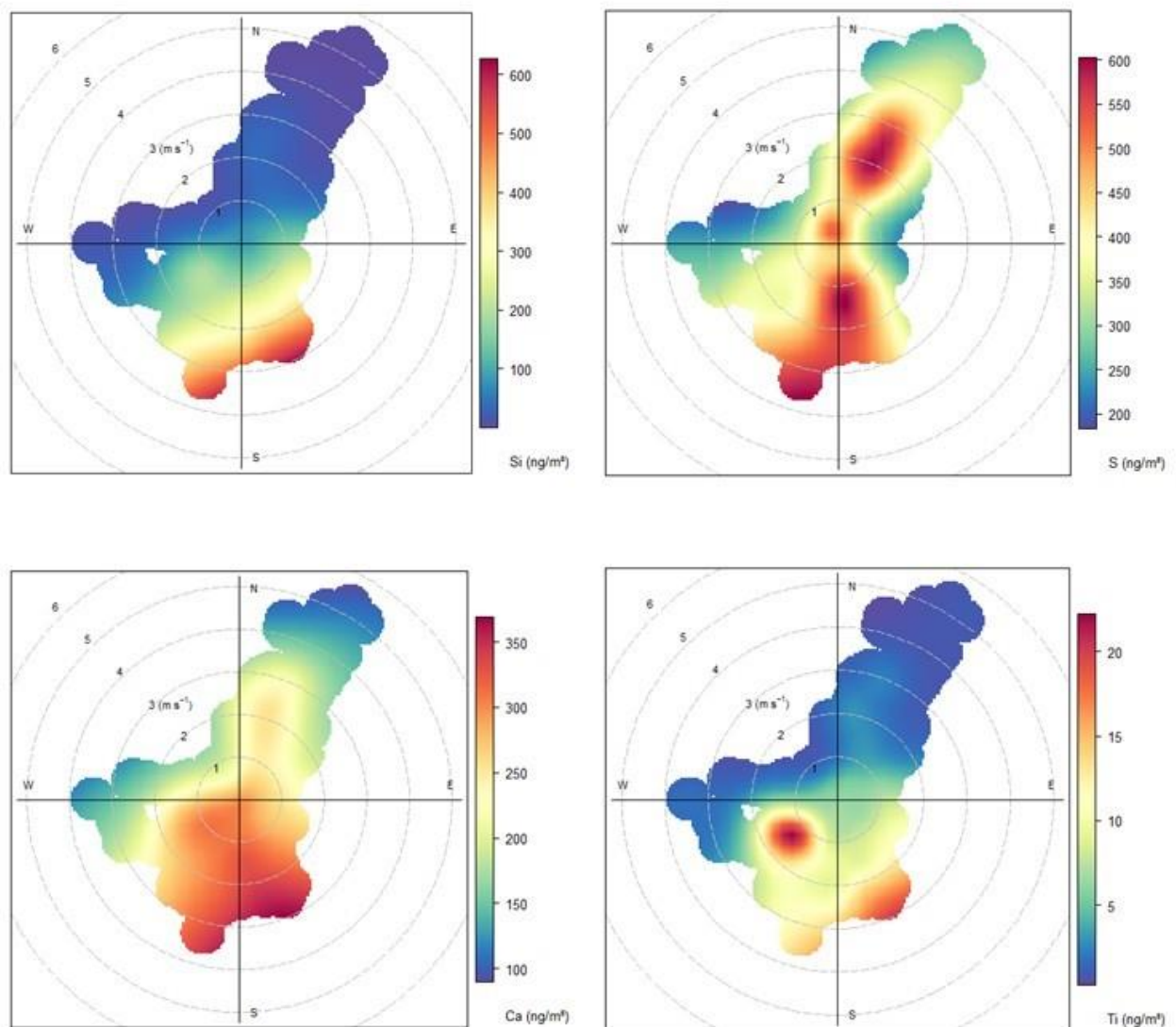


Figure 20. Pollution roses (bivariate plots) showing the distribution of Si, S, Ca, and Ti concentrations as a function of wind direction and wind speed. The radial axis represents wind speed (m/s), while the angular position indicates wind direction. The colour scale represents the concentration of the elements (ng/m<sup>3</sup>), with warmer colour (red) indicating higher concentrations.

Unlike typical crustal elements, K, Fe, Cu, and Zn show high concentration levels near the sampling point at low wind speed, as highlighted by Figure 20, suggesting a common nearby emission source.

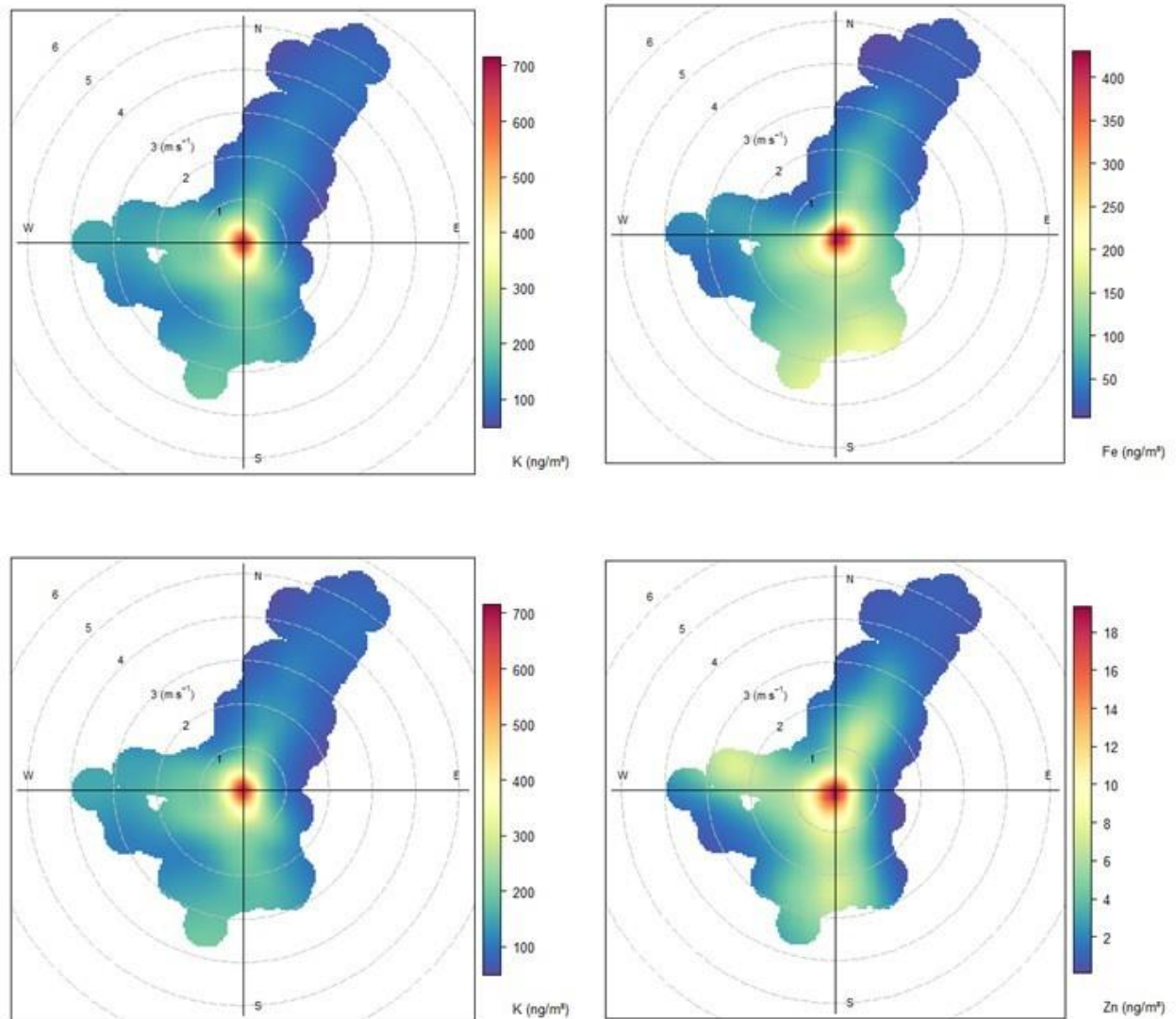


Figure 21. Pollution roses (bivariate plots) showing the distribution of K, Fe, Cu, and Zn concentrations as a function of wind direction and wind speed. The radial axis represents wind speed (m/s), while the angular position indicates wind direction. The colour scale represents the concentration of the elements ( $\text{ng}/\text{m}^3$ ), with warmer colour (red) indicating higher concentrations.

## PMF SOURCE APPORTIONMENT BASED ON MEASUREMENTS OF PARTICLE NUMBER CONCENTRATIONS AND COMPARISON WITH CHEMICAL-BASED APPORTIONMENT

Aerosol source apportionment is important to understand particulate matter (PM) sources and better define mitigation strategies to improve air quality. To this end many efforts have been made to elaborate model-based approaches exploiting PM measurements and their relevant physical and chemical properties (Hopke, 2016). Receptor models such as Positive Matrix Factorization (PMF) have been very useful to this purpose and currently represent the most widely used method for PM chemical speciation or PNSD source apportionment, as recently summarized for example in the RI-URBANS guidance document (RI-URBANS, 2024).

Over Italian sites, these approaches have been used to perform the PM source apportionment based on chemical speciation data (Pietrodangelo et al., 2024, Hopke et al., 2020, Bernardoni et al., 2011, Cesari et al., 2018), whereas few studies included apportionment based on particle size distributions (Masiol et al., 2016, Diemoz et al., 2019; Garcia-Marlès et al., 2024). In this respect, numerous studies worldwide have demonstrated the valuable insights provided using receptor modelling on size-resolved ultra-fine mode particles (UFP) data (Hopke et al., 2022) using primarily scanning mobility particle sizers (SMPS). In some cases, the PNSD analysis was extended to include accumulation and coarse modes (2.5 - 10  $\mu\text{m}$ ) typically using Aerodynamic particle sizers (APSs) (Leoni et al., 2018, Harrison et al., 2011; Masiol et al., 2016). Optical particle counters (OPCs) offer a cost-effective alternative to aerodynamic particle sizers.

For the ECO station in Lecce, some previous studies using PMF techniques made use of the PM chemical information (Giannossa, 2022), but limited attempts were done combining this information with the one derived by co-located aerosol physical measurements (e.g. PNSD and optical properties). Particle distributions in Lecce were previously studied by Dinoi et al., (2023), but source apportionment analysis of these was only recently performed by Garcia-Marlès et al. (2024), focusing on the ultrafine and accumulation modes (i.e. 0.01-0.8  $\mu\text{m}$ ).

Although the information obtained from chemical PMF analysis is comprehensive, the use of the physical information has some potential advantages. In fact, it ensures near-real-time and high time resolution measurements with relatively low resource expenses, compared to the chemical characterization which is more demanding in term of cost and human effort and offers limited temporal resolution (typically daily). In this chapter, we feed PMF with aerosol physical data and chemical analysis, namely ultrafine to coarse PNSD, ranging from 0.01-10  $\mu\text{m}$ , plus aerosol absorption, recorded at the Lecce site between 2016 and 2017. The aim of the work was to investigate a) if and how the PMF-based analysis of aerosol physical properties is effective in providing information on the aerosol sources, b) how the physics-PMF results compare to the relevant ones obtained using the chemical information, and c) what is the added value of using a combination of physical and chemical properties in the PMF-based source apportionment.

### Methods

The site of Lecce, where the ECO observatory was built, is a suburban area in the southeastern edge of the Italian peninsula, and it is influenced by both anthropogenic and natural sources. Main anthropogenic sources are vehicular traffic and biomass combustion emissions, these originating from both domestic heating and burning of agricultural residuals. Natural aerosols are mainly sea spray and crustal dust of both local and long-range transport origin (e.g. desert dust from North Africa). Occasionally, transregional transport of aerosols from large industrial complexes located approximately 30- 80 km from the site, or from Eastern Europe occurs.

In previous studies, the chemical composition of PM<sub>2.5</sub> and PM<sub>10</sub> at this site was analysed, and source apportionment was determined using the EPA PMF 5.0 model (Cesari et al., 2018, Giannossa et al., 2022). From such studies, emission sources such as traffic, biomass burning, secondary nitrate, secondary sulphate, sea spray, crustal and carbonates were clearly identified and carefully analysed.

#### Instrumentation

Information on the aerosol size distribution from the ultrafine to the coarse fraction was derived combining an Optical Particle Counter (OPC Grimm 11-A) and a Scanning Mobility Particle Sizer (SMPS, TROPOS). The OPC measured the particle number concentration in the size range from 0.25 to 10 µm working at controlled flow of 1.2 L/min. The SMPS was employed to monitor aerosol size distribution within the range between 10 nm and 800 nm.

Aerosol optical properties, and specifically the aerosol absorption coefficient, were measured by a Multi Angle Absorption Photometer (MAAP Thermo Scientific, mod. 5012). Here we use the MAAP-based equivalent black carbon (eBC) concentrations, derived from the measured aerosol absorption at 670 nm using a mass absorption coefficient (MAC) of 6.6 m<sup>2</sup>/g.

Additional information on sulfur dioxide (SO<sub>2</sub>) and nitrogen oxides (NO-NO<sub>2</sub>-NO<sub>x</sub>) was also considered, this being provided by measurements using the Thermo Instruments analyzers, TEI 43i and 42i, respectively.

Meteorological data from the ECO observatory was also used to facilitate interpretation of the results.

#### PMF analysis

The EPA PMF 5.0 tool was used to perform the PMF analysis. Positive matrix factorization is a receptor model, and as such is based on the mass conservation principle accounting for  $m$  species in the  $n$  samples as contributions from  $p$  independent sources:

$$x_{ij} = \sum_{k=1}^p g_{ik} f_{kj} + e_{ij}$$

where  $x_{ij}$  is the  $j^{\text{th}}$  species concentration measured in the  $i^{\text{th}}$  sample,  $g_{ik}$  is the contribution of the  $k^{\text{th}}$  source to  $i^{\text{th}}$  sample, and  $f_{jk}$  is the concentration of the  $j^{\text{th}}$  species in  $k^{\text{th}}$  source. Lastly,  $e_{ij}$  is the residual for each sample/species. This equation was applied to an hourly dataset of size bins spectra from SMPS+OPC plus the eBC concentration. The PMF model then uses the uncertainties measured for each size-bin or eBC concentration to weigh their contribution using the least-squares minimization. The estimation of uncertainties is therefore critical for the success of the PMF solution. In this study the uncertainties were calculated using a method formulated by Ogulei et al., 2007.

$$s_{ij} = \sigma_{ij} + (C_3 * N_{ij})$$

$$\sigma_{ij} = (\alpha) * (N_{ij} + \bar{N}_{ij})$$

where  $\sigma$  is the uncertainty estimated for an observation;  $N$  represents the observed concentration;  $\bar{N}$  is the arithmetic mean of the concentrations of each size bin;  $\alpha$  is constant (0.01);  $s$  is the overall uncertainty matrix; and lastly  $C_3$  is a constant determined by trial-and-error (0.1 for eBC and size bin

up to 1.8 mm, 0.29 for size bins from 2.2 mm up to 5.5 mm, 0.49 for the largest size bins). Q values and residual analysis and bootstrap method were used to determine the optimal number of factors.

The input dataset for the PMF analysis included size distributions measured using SMPS and OPC, along with eBC concentrations determined via MAAP. The data from all instruments were averaged on an hourly basis to ensure consistency and comparability. Unfortunately, there were gaps in the measurements, and the overlap between datasets was not continuous and the total number of days was 371. Figure 21 shows the months that were available for all datasets and the number of days for each month.

A preliminary investigation was done to understand the best configuration of the input file, together with the uncertainties and number of factors. In this report we only present and discuss the results obtained from such ‘best configuration’, this leading to a 8-factors solution having best Q values and residual analysis.

## Results

We first investigated the monthly-resolved variability of particle size distribution over the 2-year period (2016-2017). Figure 21 presents the monthly-resolved median size distribution both in terms of volume (top panels) and number (bottom panels) distributions. It shows very good continuity between SMPS and OPC sizes, this being confirmed all through the year.

As mentioned, when fed with particle size distribution plus eBC data, a PMF solution comprising eight factors provided the best results based on residual analysis (remaining consistently within +/- 3) and Q values. Figure 22 presents the profiles of each factor, named according to the size of their modal mode while Figure 23 shows the percentage contributions of eBC to each factor. The model was executed twice: first using particle number concentrations and then using particle volume concentrations. As illustrated in Figure 24, the mean percentage contributions to the total volume and total number were inversely related for ultrafine and coarse factors. Notably, the same factor profiles were obtained from both datasets, ensuring consistency in the results.

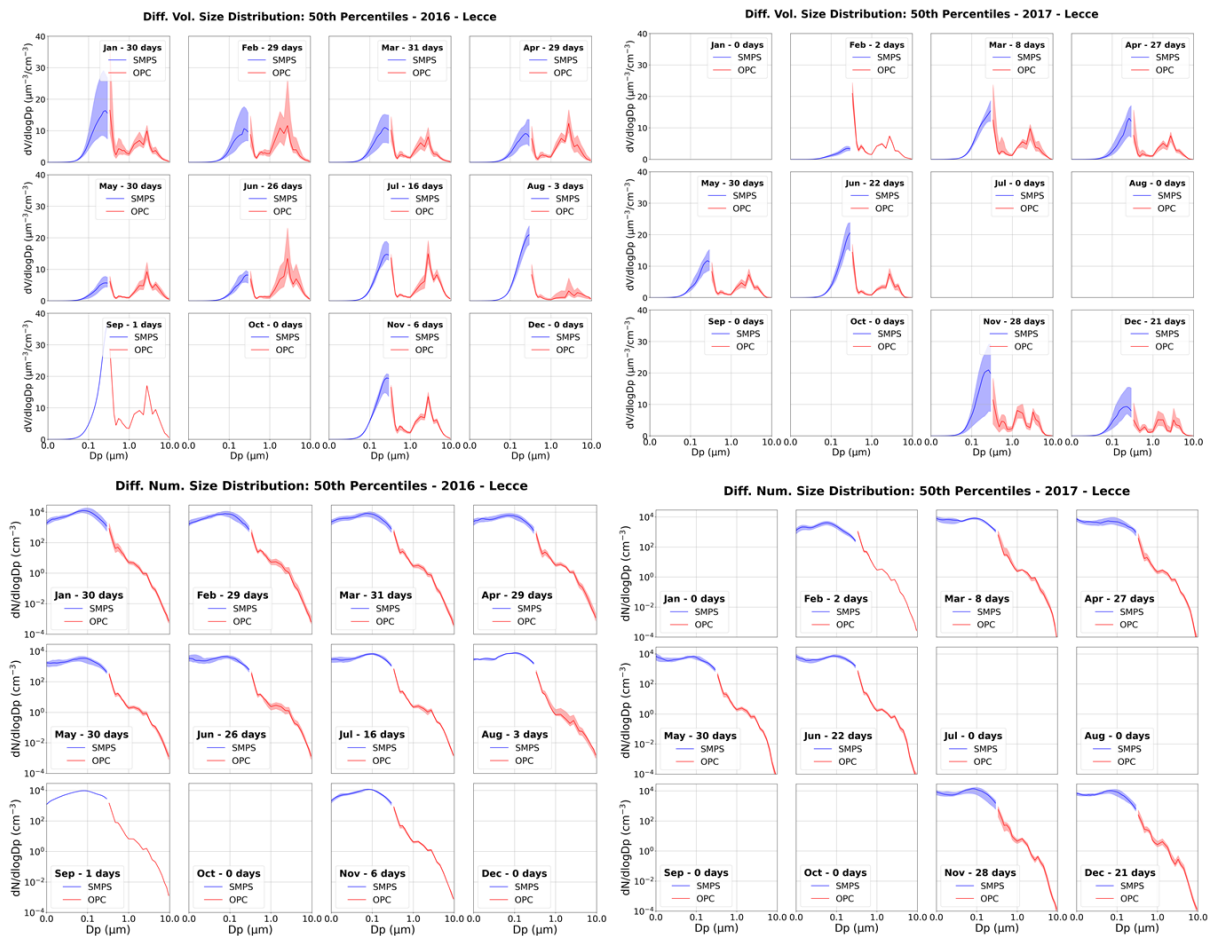


Figure 22. Monthly resolved median size distributions expressed in number (top figures) and volume (bottom figures) concentrations for the year 2016 (on the left) and 2017 (on the right) coming from SMPS (blue) and OPC (red). The shaded area represents the 25th-7

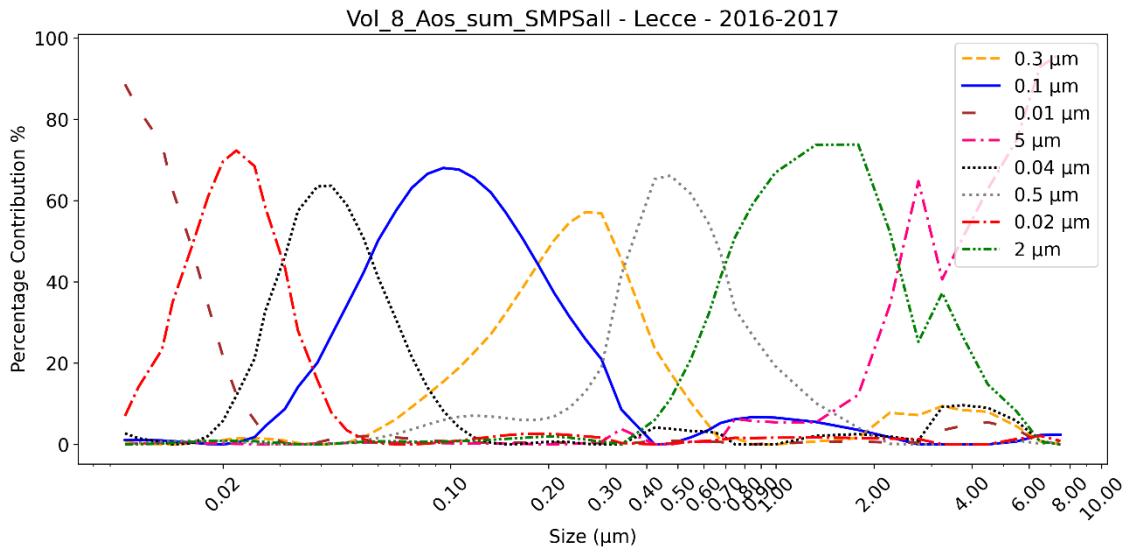


Figure 23. . Factor profiles in terms of percentage contribution to the species sum. For convenience, factor naming follows the dimension of the size bin corresponding to the modal radius.

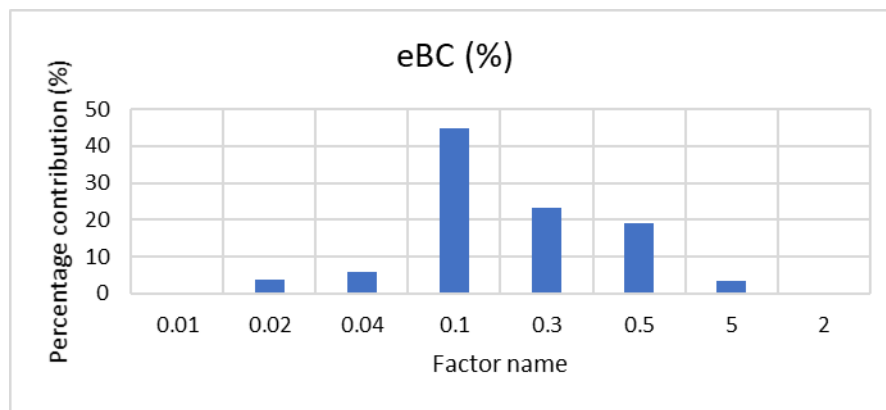


Figure 24. Percentage contribution to the total eBC for each factor.

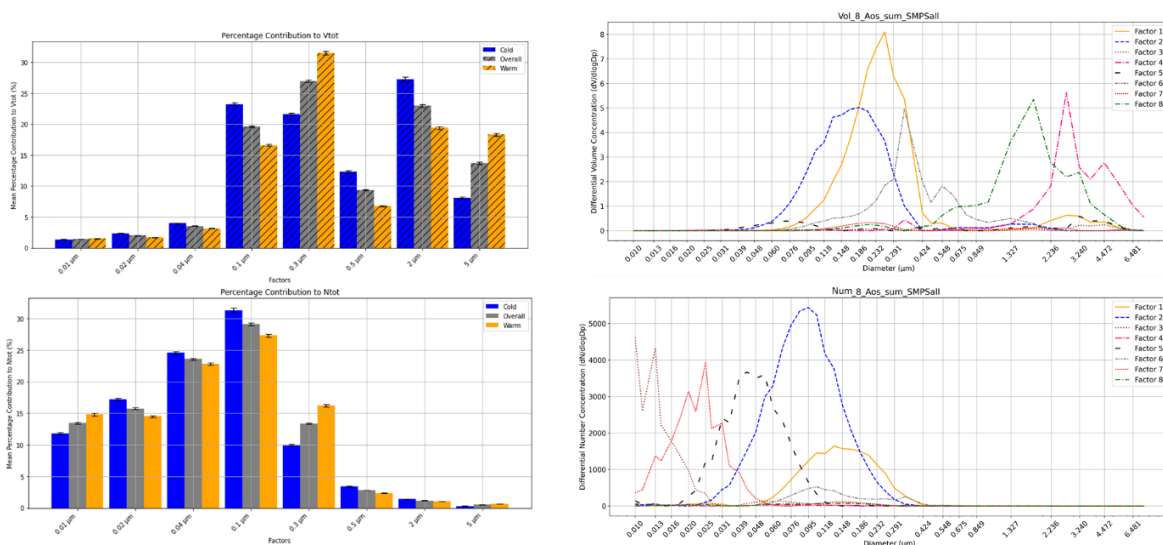


Figure 25. Bar charts display the mean percentage contribution to the total volume (top left) and total number (bottom left) of size bins across the year (grey bars), and separately for cold (October–March, blue bars) and warm (April–September, yellow bars) months. Standard error is indicated by error bars. Additionally, the figure includes particle volume (top right) and number (bottom right) distributions of the 8 factors.

The interpretation of these results in terms of aerosol sources was made thanks to the analysis of a) the factor profiles, b) of their daily, weekly and annual cycles (Figure 25), c) polar plots relating source factors to origin area through wind data (Figure 26), and c) correlation with measured trace gases. The following considerations were made:

- *Factor 0.01  $\mu\text{m}$  / Nucleation or Photonucleation:* major size mode at the detection limit of 0.01  $\mu\text{m}$ ; the diurnal trend shows a midday peak. It contributes 13.4% to the total number concentration and 1.5% to the total volume. eBC does not contribute to this profile and no correlations with trace gases were found. A polar plot reveals a strong association between elevated concentrations of this source and wind originating from the northwest.
- *Factor 0.02  $\mu\text{m}$  / Traffic-Nucleation:* dominant size mode at around 0.02  $\mu\text{m}$ . The diurnal trend shows a marked midday peak in the summer, whereas in autumn the maximum concentrations align with traffic rush hours and minimum values at the weekend. It contributes 16.4% to the total number concentration and 2.5% to the total volume. A trace quantity of eBC contributes to this source. The polar plot reveals some association between elevated concentrations of this source and wind originating from the northwest, especially in winter.
- *0.04  $\mu\text{m}$  / Traffic1:* prevailing mode at 0.04  $\mu\text{m}$ ; the diurnal trend shows maximum peaks at traffic rush hours. It contributes 24.4% to the total number concentration and 4.5% to the total volume. A small amount of eBC contributes to this factor (around 5% of the total eBC), arising some doubts over this factor assignment. However, a discrete positive correlation ( $R=0.54$ ) with  $\text{NO}_2$  concentration was observed. Seasonal polar plots show this emission source has primarily a local origin especially in autumn.
- *0.1  $\mu\text{m}$  / Traffic2-Domestic Heating-Urban Background:* major mode at around 0.1  $\mu\text{m}$ ; the diurnal trend reveals maximum peaks during traffic rush hours and extending into late evening in autumn and winter, highlighting the influence of domestic heating. This factor accounts for 29.4% of the total number concentration and 20.5% of the total volume, making it the primary contributor to number concentration. Additionally, it is responsible for approximately 50% of eBC, emphasizing its significant impact. This factor shows a positive correlation with both  $\text{NO}$  ( $R=0.56$ ) and  $\text{NO}_2$  ( $R=0.67$ ). Seasonal polar plots indicate that this source also has a primarily local origin, particularly in autumn and winter. A slight increase in concentration observed in June may be attributed to fire emissions or tourism-related traffic.
- *0.3  $\mu\text{m}$  / Secondary Sulphate:* major mode at around 0.3  $\mu\text{m}$ . The diurnal trends show a nighttime increase, with accumulation continuing until early morning. This factor contributes 13.4% to the total number concentration and 27.5% to the total volume, making it the dominant contributor to volume concentration. An increase is observed during summer, and polar plots indicate that long-range transport plays a significant role in this season.
- *0.5  $\mu\text{m}$  / Secondary Nitrate:* major mode at around 0.5  $\mu\text{m}$ . This is a winter dominating factor showing a combination of rush-hour and nighttime peaks. This factor contributes 3.4% to the total number concentration and 9.5% to the total volume, and it is a primarily local source.
- *2  $\mu\text{m}$  / Regional Transport:* major mode at around 2  $\mu\text{m}$ . As expected for transported sources, its diurnal trend shows no significant variation, though a moderate decrease in the morning and night is observed, likely due to wind shifts. This factor accounts for 1.4% of the total number concentration and 23.5% of the total volume. It is predominantly transported from the southeast.
- *5  $\mu\text{m}$  / Local resuspension:* size mode peaking around 5  $\mu\text{m}$ . In a similar although antithetical way as the previous factor, it shows a variable diurnal trend with an increase in the morning

and nighttime. This factor accounts for 1.4% of the total number concentration and 14.5% of the total volume. Seasonal polar plots indicate a variable origin during summer, consistent with dry soil emissions, while in winter, it is predominantly transported from the southeast.

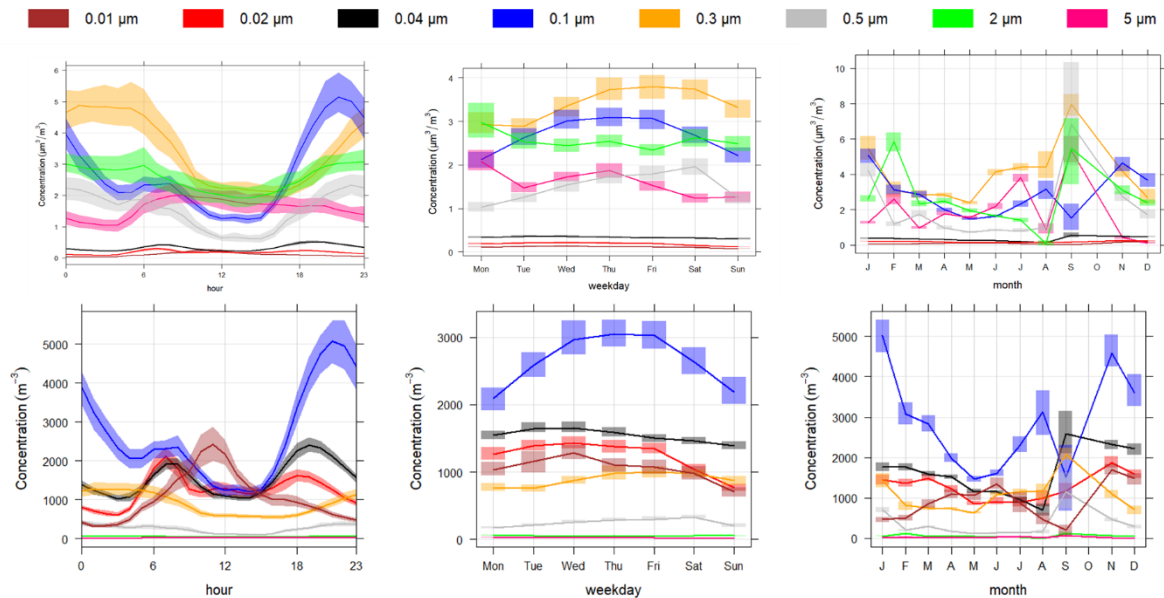


Figure 26. Hourly, weekly and daily temporal trend of the 8-factor solutions in terms of volume and number concentrations.

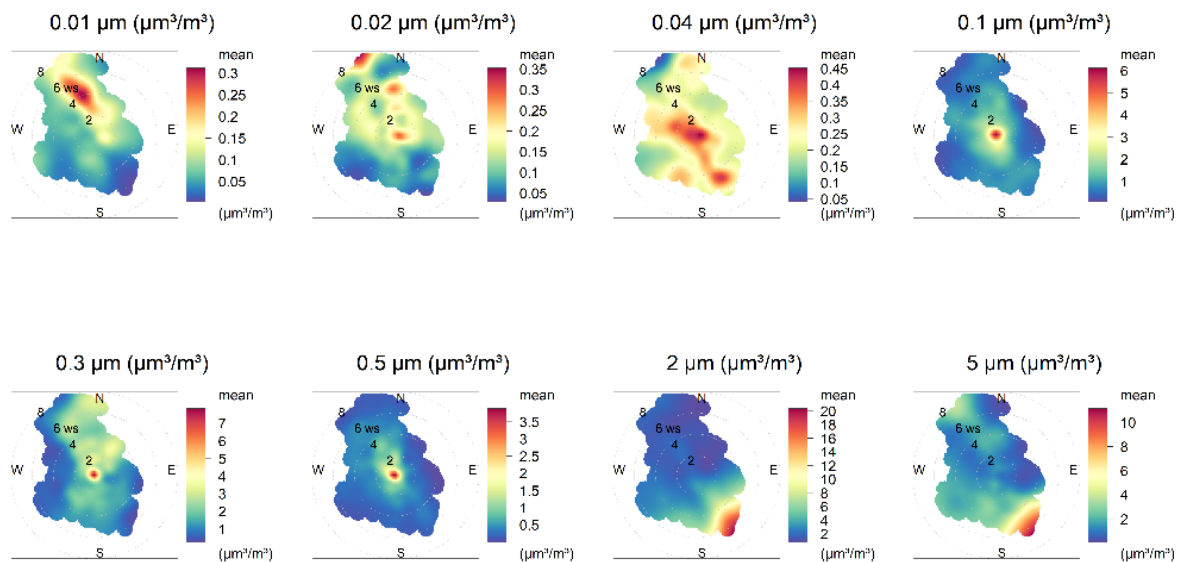


Figure 27. Polar plots for the eight PMF factors.

### Physical vs Chemical PMF

In order to perform a direct comparison between the chemical-PMF and physical-PMF, the hourly resolved physical-PMF factors were averaged to daily means. A correlation matrix was then built comparing the results to the chemical characterization of PM<sub>2.5</sub> and PM<sub>10</sub> made by Giannossa et al. (2022) (Figure 27), and the relevant chemical PMF factors (Figure 28) (traffic, biomass burning, secondary sulphate, secondary nitrate, crustal, sea spray and carbonates). Despite the scarce number of days in common between chemical and physical PMF (31 days mainly distributed over April, June, July and November 2017), the comparison between chemical- and physical-PMF provided useful insights to understand the differences of the two distinct approaches. The Table 3 below summarizes the results showing the chemical species or factors for which the correlation coefficient R was higher than 0.5.

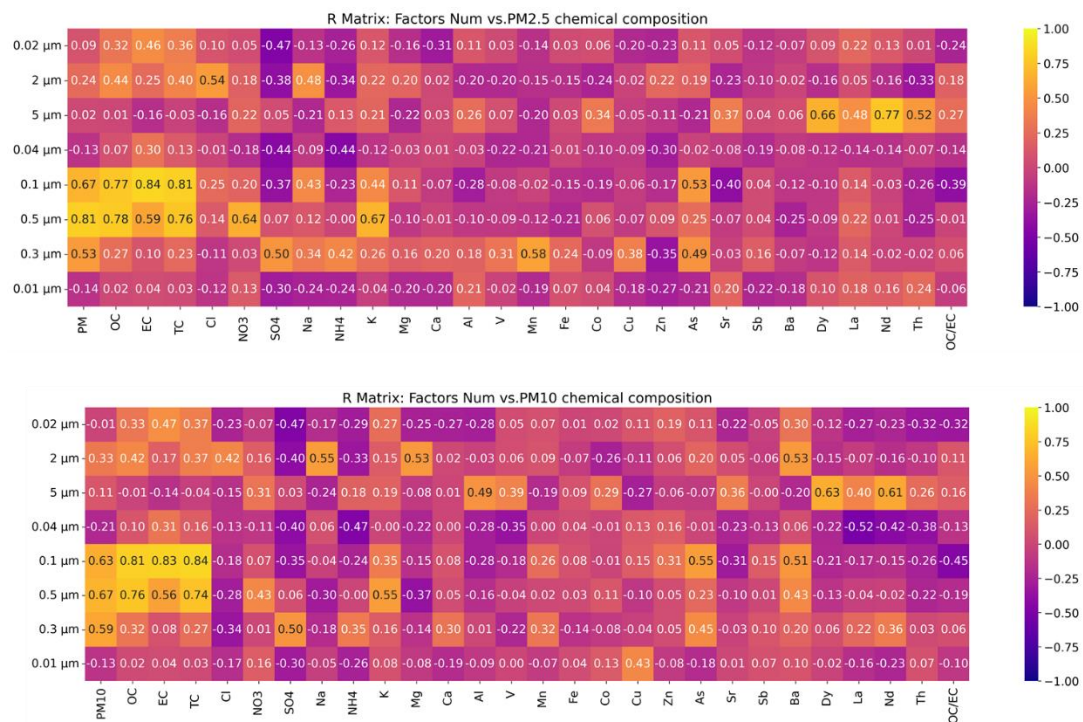


Figure 28. Correlation matrix between daily means of size-PMF factors and chemical species determined by Giannossa et al.(2022).

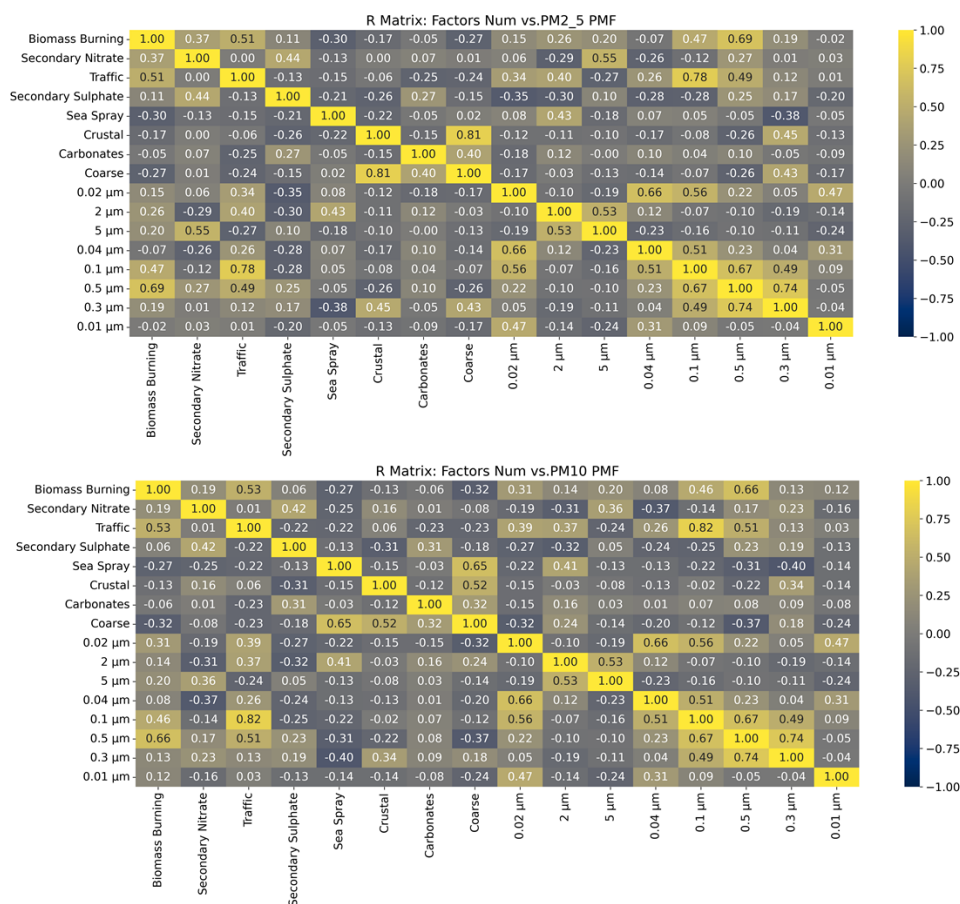


Figure 29. Correlation matrix between daily means of size-PMF factors and chemical PMF factors determined by Giannossa et al.(2022).

Physical PMF factors	0.01 μm	0.02 μm	0.04 μm	0.1 μm	0.3 μm	0.5 μm	2 μm	5 μm
Names	<i>Photo-nucleation</i>	<i>Nucleation</i>	<i>Traffic1</i>	<i>Traffic2/Do mestic heating</i>	<i>Secondary Sulphate</i>	<i>Secondary Nitrate</i>	<i>Regional Transport</i>	<i>Local Resuspension</i>
Chemical species PM2.5	-	-	-	EC, OC	SO <sub>4</sub> , Mn	EC, OC, K, NO <sub>3</sub>	Na, Cl	Dy, Nd, Th
Chemical species PM10	-	-	-	EC, OC	SO <sub>4</sub>	EC, OC, K	Na, Cl	Dy, Nd
Chemical PMF factors PM2.5	-	-	-	Traffic	-	BB	-	-
Chemical PMF factors PM10	-	-	-	Traffic	-	BB, Traffic	-	-

Table 3. Chemical species and chemical PMF factors correlating with size-PMF factors with R≥0.5.

The ultrafine mode factors exhibit no correlation coefficients higher than 0.5, highlighting how the focus on  $PM_{2.5}$  and  $PM_{10}$  leads to a loss of critical information regarding particles in the ultrafine range. Another observation is that correlation with chemical species gives more insight than the correlation with whole PMF factors, which shows significant results only for the factors traffic and biomass burning. On the other hand, the correlations between chemical species and factors confirmed some of the physical PMF assignment such as the secondary sulphate to the 0.3  $\mu m$  factor ( $R_{PM_{2.5}} = 0.5$ ) and the secondary nitrate to the 0.5  $\mu m$  factor ( $R_{PM_{2.5}}=0.64$ ). The correlation of 0.3  $\mu m$  factor with organic carbon ( $R_{PM_{2.5}}=0.78$ ) and with K ( $R_{PM_{2.5}}=0.67$ ) suggests the contribution of biomass burning emissions to this source. The correlation with Na and Cl with the 2  $\mu m$  factor gives information about the composition of this coarse factor ( $R_{PM_{10}} =0.5$ ), which is likely a mixture of crustal dust and sea spray, an occurrence that is not uncommon in this region.

## Summary

As detailed in the introduction, this study aimed at exploring the potential use of the aerosol physical properties information collected at ECO station in Lecce to feed a PMF model and derive main aerosol source factors, comparing and comparing the results to the ones obtained by chemical-PMF. Main results can be summarized as follows:

- a) the dataset based on aerosol physical properties such as size distributions from SMPS and OPC (0.01-10  $\mu m$ ) and eBC concentration from MAAP represent a valid PMF model input. Preliminary studies showed a promising solution of 8 factors that are still under investigation. An initial analysis led to the identification of three ultra-fine mode sources related to photo nucleation, nucleation and traffic. However, the low presence of eBC raises some doubts regarding this interpretation. The largest contribution to number concentration was recorded for another ultra-fine factor possibly related to traffic, even though the temporal trend would suggest also the involvement of domestic heating to this source. Two secondary sources were assigned to nitrate and sulphate rich particles, with the nitrate source being likely linked also to biomass burning emissions. And lastly two coarse mode sources were identified as regional transport and local resuspension, where regional transport is likely to include sea-spray emissions.
- b) Comparing physical and chemical information is a useful tool for the interpretation of PMF results. Daily means of the physical PMF factors were compared to chemical PMF factors and chemical speciation. Even though the first ultra-fine mode factors were not correlated with any of the chemical PMF factors or species, the other factors showed interesting correlations especially with chemical species. In fact, both secondary factors correlated with sulphate and nitrate ions, and the secondary nitrate was also correlated with OC, K and biomass burning factor, suggesting biomass burning contribution. The traffic source was correlated to EC and OC and the chemical traffic factor. The regional transport was correlated to Na and Cl, but not with the sea-spray chemical factor. Overall, the comparison with chemical species proved more insightful than the comparison with chemical PMF factors. It played a crucial role in validating the interpretations derived from the physical data, while also enriching the analysis in certain cases by providing additional information.
- c) Several advantages come from the use of physical properties for source apportionment, such as quasi real-time monitoring, relative ease of instrument use, and ultra-fine particles observation. However, sources where particle number concentration dominates sometimes differ from sources where the particulate matter mass concentration prevails. In this sense

the synergic approach of physical and chemical characterization is key to the study of aerosol and aerosol sources.

A further future optimization of the physical-PMF model focusing will consider the following steps:

- Uncertainty optimization: the estimation of the uncertainties is crucial for the PMF model, and more efforts will be directed in this direction to find the optimal values for this dataset.
- Trace gases: Incorporating trace gases directly into the input dataset could yield more valuable insights compared to relying solely on ‘a posteriori’ correlation analyses and it is recommended in the RI-URBANS guidelines for source apportionment.
- Seasonal analysis: separating the dataset by season could be a great improvement considering the limit of operating the EPA PMF 5.0 with large input datasets, which make it hard to perform the displacement and bootstrap analysis on our full dataset.
- A more careful analysis of case studies will be performed combining the PMF-outcome to aerosol typing based on independent dataset from remote-sensing data, (including satellite observations, photometric measurements or vertical profiling by lidar/ceilometers).

## CONCLUSIONS

The report shows how the new instruments that have been installed and made operative at ECO station can be used for source identification and characterization suggesting the potentiality of high temporal resolution in source apportionment. Different instruments measuring absorption furnish well comparable results when harmonized using site-specific MAC values and are able The offline mixing of size distributions from SMPS, OPC, with chemical tracers allows a better understanding of the impact of specific sources including nucleation. Future developments will include the use of receptor models applied to longer dataset at high temporal resolution that could be the base for development of near-real-time characterization of PM sources.

## REFERENCES

- Andreae, M.O., Gelencsér, A., 2006. Black carbon or brown carbon? The nature of light-absorbing carbonaceous aerosols, *Atmos. Chem. Phys.* 6, 3131–3148.
- Bernardoni, V., Vecchi, R., Valli, G., Fermo, P., Piazzalunga, A., & Prati, P., 2011. Fine carbonaceous particulate matter in the Alpine region: Local and long-range contributions. *Science of the Total Environment* 409, 2260–2268.
- Bond, T.C., Habib, G., Bergstrom, R.W., 2006. Limitations in the enhancement of visible light absorption due to mixing state. *J. Geophys. Res.* 111, D20211.
- Bond, T.C., Bergstrom, R.W., 2006. Light absorption by carbonaceous particles: an investigative review. *Aerosol. Sci. Technol.* 40 (1), 27-67.
- Bond, T.C., Doherty, S.J., Fahey, D.W., Forster, P.M., Berntsen, T., DeAngelo, B.J., Flanner, M.G., Ghan, S., Kärcher, B., Koch, D., Kinne, S., Kondo, Y., Quinn, P.K., Sarofim, M.C., Schultz, M.G., Schulz, M., Venkataraman, C., Zhang, H., Zhang, S., Bellouin, N., Guttikunda, S.K., Hopke, P.K., Jacobson, M.Z., Kaiser, J.W., Klimont, Z., Lohmann, U., Schwarz, J.P., Shindell, D., Storelvmo, T., Warren, S.G., Zender, C.S., 2013. Bounding the role of black carbon in the climate system: a scientific assessment. *J. Geophys. Res. Atmos.* 118, 5380–5552.

Cesari D., Merico E., Dinoi A., Marinoni A., Bonasoni P., Contini D., 2018a. Seasonal variability of carbonaceous aerosols in an urban background area in Southern Italy. *Atmospheric Environment*, 200, 97–108.

Cesari, D., Donato, A., Contini, D., & Conte, M., 2018b. Seasonal variability of PM<sub>2.5</sub> and PM<sub>10</sub> composition and sources in an urban background site in Southern Italy. *Science of the Total Environment* 612, 202–213.

Chow, J. C., Watson, J. G., Chen, L.W.A., Arnott, W.P., Moosmuller, H., Fung, K., 2004. Equivalence of elemental carbon by thermal/ optical reflectance and transmittance with different temperature protocols. *Environ Sci Technol.* 38(16):4414-22.

Daellenbach, K.R., Uzu, G., Jiang, J., Cassagnes, L.-E., Leni, Z., Vlachou, A., Stefenelli, G., Canonaco, F., Weber, S., Segers, A., Kuenen, J.J.P., Schaap, M., Favez, O., Albinet, A., Aksoyoglu, S., Dommen, J., Baltensperger, U., Geiser, M., El Haddad, I., Jaffrezo, J.-L., Prévôt, A.S.H., 2020. Sources of particulate-matter air pollution and its oxidative potential in Europe. *Nature* 587, 414–419.

Diemoz et al., 2019. Transport of Po Valley aerosol pollution to the northwestern Alps – Part 2: Long-term impact on air quality. *Atmospheric Chemistry and Physics* 19, 10129–10129.

Dinoi A., Cesari D., Marinoni A., Bonasoni P., Riccio A., Chianese E., Tirimberio G., Naccarato A., Sprovieri F., Andreoli, V., Moretti, S., Gulli D., Calidonna C.R., Ammoscato I., Contini D., 2017. Inter-comparison of carbon content in PM<sub>2.5</sub> and PM<sub>10</sub> collected at five measurement sites in southern Italy. *Atmosphere*, 8 (12), 243.

Dinoi, A., Baldassarre, F., Fermo, P., et al., 2023. Characterization of ultrafine particles and the occurrence of new particle formation events in an urban and coastal site of the Mediterranean area. *Atmospheric Chemistry and Physics* 23(3), 2167–2181.

Garcia-Malès, A., Harrison, R. M., Beddows, D., et al., 2024. Source apportionment of ultrafine particles in urban Europe. *Environmental International* 194, 109149.

Giannossa, L. C., Manigrasso, M., Avino, P., et al., 2022. Inter-annual variability of source contributions to PM<sub>10</sub>, PM<sub>2.5</sub>, and oxidative potential in an urban background site in the central Mediterranean. *Journal of Environmental Management* 319, 115752.

Harrison, R. M., Beddows, D. C. S., & Dall’Osto, M., 2011. PMF Analysis of Wide-Range Particle Size Spectra Collected on a Major Highway. *Environmental Science & Technology* 45(13), 5522–5528.

Hopke, P. K., 2016. Review of receptor modeling methods for source apportionment. *Journal of the Air & Waste Management Association* 66(7), 613–615.

Hopke, P. K., Dai, Q., Li, L., et al., 2020. Global review of recent source apportionments for airborne particulate matter. *Science of the Total Environment* 703, 140091.

Hopke, P. K., Leoni, C., Paglione, M., et al., 2022. Source apportionment of particle number concentrations: A global review. *Science of the Total Environment* 807, 153104.

Kanakidou, M., Seinfeld, J.H., Pandis, S.N., Barnes, I., Dentener, F.J., Facchini, M.C., Van Dingenen, R., Ervens, B., Nenes, A., Nielsen, C.J., Swietlicki, E., Putaud, J.P., Balkanski, Y., Fuzzi, S., Horth, J., Moortgat, G.K., Winterhalter, R., Myhre, C.E.L., Tsigaridis, K., Vignati, E., Stephanou, E.G., Wilson, J., 2005. Organic aerosol and global climate modelling: A review. *Atmos. Chem. Phys.* 5: 1053–1123.

Ivančič M., Gregorič A., Lavrič G., Alföldy B., Ježek I., Hasheminassab S., Pakbin P., Ahangar F., Sowlat M., Boddeker S., Rigler M., 2022. Two-year-long high-time-resolution apportionment of primary and secondary carbonaceous aerosols in the Los Angeles Basin using an advanced total carbon–black carbon (TC-BC( $\lambda$ )) method. *Science of The Total Environment*, 848, 157606.

IPPC, 2013. Climate change 2013: the physical science basis. In: Stocker, T.F., Qin, D., Plattner, G.K., Tignor, M., Allen, S.K., Boschung, J., Nauels, A., Xia, Y., Bex, V., Midgley, P.M. (Eds.), Fifth Assessment Report of the Intergovernmental Panel on Climate Change. Cambridge University Press, Cambridge, United Kingdom and New York, NY, USA, p. 1535.

Leoni, C., Conte, M., Donato, A., et al., 2018. Source apportionment of aerosol particles at a European air pollution hot spot using particle number size distributions and chemical composition. *Environmental Pollution* 233, 174–183.

Liu, D., Flynn, M., Gysel, M., Targino, A., Crawford, I., Bower, K., Choularton, T., Juranyi, Z., Steinbacher, M., Hüglin, C., Curtius, J., Kampus, M., Petzold, A., Weingartner, E., Baltensperger, U., Coe, H., 2010. Single particle characterization of black carbon aerosols at a tropospheric alpine site in Switzerland. *Atmos. Chem. Phys.* 10 (15), 7389-7407.

Liu, S., Aiken, A.C., Gorkowski, K., Dubey, M.K., Cappa, C.D., Williams, L.R., Herndon, S.C., Massoli, P., Fortner, E.C., Chhabra, P. S., Brooks, W. A., Onasch, T. B., Jayne, J.T., Worsnop, D.R., China, S., Sharma, N., Mazzoleni, C., Xu, L., Ng, N.L., Liu, D., Allan, J.D., Lee, J.D., Fleming, Z.L., Mohr, C., Zotter, P., Szidat, S., and Prévôt, A.S.H., 2015. Enhanced light absorption by mixed source black and brown carbon particles in UK winter. *Nat. Commun.* 6, 8435.

Massabò D., Prati P., 2021. An overview of optical and thermal methods for the characterization of carbonaceous aerosol. *La Rivista del Nuovo Cimento* (2021) 44:145–192.

Merico, E., Cesari, D., Dinoi, A., Gambaro, A., Barbaro, E., Guascito, M.R., Giannossa, L.C., Mangone, A., Contini, D., 2019. Inter-comparison of carbon content in PM10 and PM2.5 measured with two thermo-optical protocols on samples collected in a Mediterranean site. *Environ Sci Pollut Res* 26, 29334–29350.

Pandolfi, M., Cusack, M., Alastuey, A., Querol, X., 2011. Variability of aerosol optical properties in the Western Mediterranean Basin. *Atmos. Chem. Phys.* 11 (15), 8189-8203.

Perrino, C., Tiwari, S., Catrambone, M., Dalla Torre, S., Rantica, E., & Canepari, S. (2011). Chemical characterisation of atmospheric PM in Delhi, India, during different periods of the year including Diwali festival. *Atmospheric Pollution Research*, 2(4), 418-427.

Pietrodangelo, A., Bernardoni, V., Fermo, P., et al., 2024. A PM10 chemically characterized nationwide dataset for Italy. Geographical influence on urban air pollution and source apportionment. *Science of the Total Environment* 908, 167891.

Putaud, J.P., Van Dingenen, R., Alastuey, A., Bauer, H., Birmili, W., Cyrys, J., Flentje, H., Fuzzi, S., Gehrig, R., Hansson, H.C., Harrison, R.M., Herrmann, H., Hitenberger, R., Hüglin, C., Jones, A.M., Kasper-Giebl, A., Kiss, G., Kousa, A., Raesa, F., 2010. A European aerosol phenomenology 3: Physical and chemical characteristics of particulate matter from 60 rural, urban, and kerbside sites across Europe. *Atmos. Environ.* 44: 1308–1320.

RI-URBANS Project, 2024. Guidance document for urban air quality monitoring. [https://riurbans.eu/wp-content/uploads/2024/11/ENV\\_GUIDANCE-DOCUMENT\\_ST11\\_SA\\_BC\\_UFP\\_OP\\_VOCs\\_Definitive.pdf](https://riurbans.eu/wp-content/uploads/2024/11/ENV_GUIDANCE-DOCUMENT_ST11_SA_BC_UFP_OP_VOCs_Definitive.pdf)

Savadkoobi, M., Pandolfi, M., Reche, C., Niemi, J.V., Mooibroek, D., Titos, G., Green, D.C., Tremper, A.H., Hueglin, C., Liakakou, E., Mihalopoulos, N., Stavroulas, I., Artíñano, B., Coz, E., Alados-Arboledas, L., Beddows, D.C., Riffault, V., de Brito, J.F., Bastian, S., Baudic, A., Colombi,

C., Costabile, F., Chazeau, B., Marchand, N., Luis Gómez-Amo, J., Estellés, V., Matos, V., van der Gaag, E., Gille, G., Luoma, K., Manninen, H.E., Norman, M., Silvergren, S., Petit, J., Putaud, J., Rattigan, O.V., Timonen, H.J., Tuch, T., Merkel, M., Weinhold, K., Vratolis, S., Vasilescu, J., Favez, O., Harrison, R.M., Laj, P., Wiedensohler, A., Hopke, P.K., Petäjä, T., Alastuey, A., Querol, X., 2023. The variability of mass concentrations and source apportionment analysis of equivalent black carbon across urban Europe. *Environment international* 178, 108081.

Savadkoohi, M., Pandolfi, M., Favez, O., Putaud, J.-P., Eleftheriadis, K., Fiebig, M., Hopke, P.K., Laj, P., Wiedensohler, A., Alados-Arboledas, L., Bastian, S., Chazeau, B., María, Á.C., Colombi, C., Costabile, F., Green, D.C., Hueglin, C., Liakakou, E., Luoma, K., Listrani, S., Mihalopoulos, N., Marchand, N., Močnik, G., Niemi, J.V., Ondráček, J., Petit, J.-E., Rattigan, O. V., Reche, C., Timonen, H., Titos, G., Tremper, A.H., Vratolis, S., Vodička, P., Funes, E.Y., Zíková, N., Harrison, R.M., Petäjä, T., Alastuey, A., Querol, X., 2024. Recommendations for reporting equivalent black carbon (eBC) mass concentrations based on long-term pan-European in-situ observations. *Environ. Int.* 185, 108553.

Sun, J. Y., Wu, C., Wu, D., Cheng, C., Li, M., Li, L., Deng, T., Yu, J. Z., Li, Y. J., Zhou, Q., Liang, Y., Sun, T., Song, L., Cheng, P., Yang, W., Pei, C., Chen, Y., Cen, Y., Nian, H., and Zhou, Z., 2020. Amplification of black carbon light absorption induced by atmospheric aging: temporal variation at seasonal and diel scales in urban Guangzhou, *Atmos. Chem. Phys.* 20, 2445–2470.

Tomašek, I., Damby, D.E., Andronico, D., Baxter, P.J., Boonen, I., Claeys, P., Denison, M.S., Horwell, C.J., Kervyn, M., Kueppers, U., Romanias, M.N., Elskens, M., 2021. Assessing the biological reactivity of organic compounds on volcanic ash: implications for human health. *Bull. Volcanol.* 83, 30.

Vörösmarty, J., Harrison, R. M., Maenhaut, W., et al., 2024. Attribution of aerosol particle number size distributions to main sources using an 11-year urban dataset. *Atmospheric Chemistry and Physics* 24, 5695–5712.

WHO, 2021. WHO Global Air Quality Guidelines: Particulate Matter (PM<sub>2.5</sub> and PM<sub>10</sub>), Ozone, Nitrogen Dioxide, Sulfur Dioxide and Carbon Monoxide. World Health Organization.

Yuan, J., Modini, R.L., Zanatta, M., Herber, A.B., Müller, T., Wehner, B., Poulain, L., Tuch, T., Baltensperger, U., and Gysel-Beer, M., 2021. Variability in the mass absorption cross section of black carbon (BC) aerosols is driven by BC internal mixing state at a central European background site (Melpitz, Germany) in winter. *Atmos. Chem. Phys.* 21, 635–655.

Zanatta, M., Gysel, M., Bukowiecki, N., Müller, T., Weingartner, E., Areskoug, H., Fiebig, M., Yttri, K.E., Mihalopoulos, N., Kouvarakis, G., Beddows, D., Harrison, R. M., Cavalli, F., Putaud, J.P., Spindler, G., Wiedensohler, A., Alastuey, A., Pandolfi, M., Sellegri, K., Swietlicki, E., Jaffrezo, J.L., Baltensperger, U., and Laj, P., 2016. A European aerosol phenomenology-5: Climatology of black carbon optical properties at regional background sites across Europe. *Atmos. Environ.* 145, 346–364.